The thermal properties of hydrothermally altered andesites from La Soufrière de Guadeloupe (Eastern Caribbean)

Michael J Heap, David Jessop, Fabian B Wadsworth, Marina Rosas-Carbajal, Jean-Christophe Komorowski, H Albert Gilg, Nadège Aron, Margaux Buscetti, Laura Gential, Margaux Goupil, et al.

The thermal properties of hydrothermally altered andesites from La Soufrière de Guadeloupe (Eastern Caribbean)

Michael J. Heap[1,2]*, David E. Jessop[3,4,5], Fabian B. Wadsworth[6], Marina Rosas-Carbajal[3], Jean-Christophe Komorowski[3], H. Albert Gilg[7], Nadège Aron[1], Margaux Buscetti[1], Laura Gential[1], Margaux Goupil[1], Mathilde Masson[1], Lucie Hervieu[1], Alexandra R.L. Kushnir[1], Patrick Baud[1], Lucille Carbillet[1], Amy G. Ryan[8], and Roberto Moretti[3,4]

[1] *Université de Strasbourg, CNRS, Institut Terre et Environnement de Strasbourg, UMR 7063, 5 rue Descartes, Strasbourg F-67084, France*

[2] *Institut Universitaire de France (IUF), Paris, France*

[3] *Université de Paris, Institut de Physique du Globe de Paris, CNRS UMR 7154, F-75005 Paris, France*

[4] *Observatoire Volcanologique et Sismologique de Guadeloupe, Institut de Physique du Globe de Paris, F-97113 Gourbeyre, France*

[5] *CNRS, IRD, OPGC Laboratoire Magmas et Volcans, Université Clermont Auvergne, F-63000, Clermont-Ferrand, France*

[6] *Earth Science, Durham University, Science Labs, Durham, DL1 3LE, United Kingdom*

[7] *Engineering Geology, TUM School of Engineering and Design, Technical University of Munich, 80333 Munich, Germany*

[8] *Department of Earth and Environmental Sciences, University of Minnesota, MN 55455, USA*

*Corresponding author: Michael Heap (heap@unistra.fr)

Abstract

The heat flux of an active volcano provides crucial information on volcanic unrest. The hydrothermal activity often responsible for volcanic unrest can be accompanied by an increase in the extent and intensity of hydrothermal alteration, which could influence the thermal properties of the volcanic edifice. Therefore, an understanding of the influence of alteration on the thermal properties of rocks is required to better interpret volcano heat flux data. We provide laboratory measurements of thermal conductivity, thermal diffusivity, and specific heat capacity for variably altered (intermediate to advanced argillic alteration) andesites from La Soufrière de Guadeloupe (Eastern Caribbean). We complement these data with previously published data for altered basaltic-andesites from Merapi (Indonesia) and new data for altered rhyodacites from Chaos Crags (USA). Our data show that thermal conductivity and thermal diffusivity decrease as a function of increasing porosity, whereas the specific heat capacity does not change systematically. Thermal conductivity decreases as a function of alteration (the percentage of secondary minerals) for the rocks from La Soufrière and Merapi (from ~1.6 to ~0.6 $W \cdot m^{-1} \cdot K^{-1}$ as alteration increases from ~1.5 to >75 wt.%), but increases for the rocks from Chaos Crags (from ~1.1 to ~1.5 $W \cdot m^{-1} \cdot K^{-1}$ as alteration increases from ~6 to ~15 wt.%). Although the thermal diffusivity of the rocks from Chaos Crags increases from ~0.65 to ~0.75−0.95 $mm^2 \cdot s^{-1}$ as alteration increases from ~6 to ~15 wt.%, the thermal diffusivity of the rocks from La Soufrière and Merapi does not appear to be greatly influenced by alteration. The specific heat capacity is not significantly affected by alteration, although there is a slight trend of increasing specific heat capacity with alteration for the rocks from La Soufrière. We conclude that the decrease in thermal conductivity as a function of alteration in the rocks from La Soufrière and Merapi is the result of the low conductivity of the secondary mineral assemblage, and that a combination of the high thermal conductivity of cristobalite and the reduction in porosity as a result of the void-filling mineral precipitation can explain the increase in thermal conductivity in the rocks from Chaos Crags. Calculations show that an increase in alteration of

a dome or edifice can result in decreases and increases in heat flow density, depending on the type of alteration. Therefore, alteration-induced changes in the thermal properties of dome or edifice rocks should be considered when interpreting volcano heat flux data. We conclude that it is important not only to monitor the extent and evolution of alteration at active volcanoes, but also the spatial distribution of alteration type.

Keywords: heat flux; alteration; porosity; thermal conductivity; thermal diffusivity; specific heat capacity; Merapi; Chaos Crags

Highlights:

- Hydrothermal alteration changes the thermal properties of volcanic rocks.
- Alteration can increase or decrease thermal properties, depending on alteration type.
- Alteration can change the conductive heat flow density at a volcano.
- Alteration should be considered when interpreting volcano heat flux data.

1 Introduction

Active volcanoes, and particularly those with very active hydrothermal systems, emit a prodigious amount of heat (Wright and Flynn, 2004). The heat from magma at depth is transported to the surface by a combination of mechanisms, including the movement of magma, the advection (e.g., by convection) of hot fluids, and the conduction of heat through rock. Because changes in the heat emitted by a volcano can indicate the movement of magma and/or modifications to the hydrothermal system, monitoring heat flux at active volcanoes provides crucial information on volcanic activity and unrest (Jessop et al., 2021). Indeed, heat flux has been measured, or is continuously monitored, at volcanoes worldwide (Dehn et al., 2001; Wright et al., 2004), including Whakaari (New Zealand; Bloomberg et al., 2014), Vulcano

(Italy; Mannini et al., 2019), Campi Flegrei (Italy; Chiodini et al., 2005), Kīlauea (USA; Harris et al., 2001), Mt Etna (Italy; Harris et al., 1997), Volcán de Colima (Mexico; Stevenson and Varley, 2008), Lascar (Chile, Wooster and Rothery, 1997), and La Soufrière de Guadeloupe (Eastern Caribbean; Jessop et al., 2021). The link between the thermal output of a volcano and volcanic activity was recently emphasised by Girona et al. (2021), who highlighted that large-scale thermal unrest was a reliable indicator of impending magmatic and phreatic eruptions.

The thermal properties of volcanic rocks comprising the edifice or dome, and processes that increase or decrease these properties, are therefore informative for those charged with interpreting surficial heat flux data at volcanoes. Furthermore, the thermal properties of volcanic rocks are also an important input parameter in a wide range of models, such as those designed to model heat loss from magma chambers, conduits, sills, dykes, lavas, and ignimbrites (Irvine, 1970; Norton and Knight, 1977; Carrigan, 1984; Bruce and Huppert, 1989; Carrigan et al., 1992; Fialko and Rubin, 1999; Wooster et al., 1997; Annen et al., 2008; Nabelek et al., 2012; Heap et al., 2017a; Annen, 2017; Mattsson et al., 2018; Tsang et al., 2019). In general, for simplicity, the thermal properties of rocks in and around volcanoes are often taken to be constant, which facilitates calculations of heat flow and how it changes with, for example, hydrothermal circulation or magma movement. And yet, laboratory data show that thermal properties are variable with porosity (e.g., Robertson and Peck, 1974) and temperature (e.g., Whittington et al., 2009).

For the reasons given above, there is a clear outstanding need to better understand the evolution of thermal properties as other rock characteristics change. This endeavour is well suited to laboratory investigation in which the thermal properties of volcanic rocks are constrained (Horai et al., 1970; Fujii and Osako, 1973; Robertson and Peck, 1974; Bagdassarov and Dingwell, 1994; Whittington et al., 2009; Romine et al., 2012; Mielke et al., 2015, 2016, 2017; Vélez et al., 2018; Heap et al., 2020a; Weydt et al., 2021). For example, the thermal

conductivity of variably porous basalt from Hawai'i (USA) was found to decrease from ~1.7 $W \cdot m^{-1} \cdot K^{-1}$ at a porosity ~0.05 down to ~0.2 $W \cdot m^{-1} \cdot K^{-1}$ at a porosity of ~0.85 (Robertson and Peck, 1974). The average thermal conductivities of andesite (average porosity of 0.095) and rhyolite lava (average porosity of 0.275) from the Tauhara geothermal field (New Zealand) were measured to be 1.32 and 1.11 $W \cdot m^{-1} \cdot K^{-1}$, respectively (Mielke et al., 2015), and the thermal conductivities of andesite (porosity of 0.023–0.130), dacite (porosity of 0.108), and rhyolite (porosity of 0.231) from the Taupō Volcanic Zone (New Zealand) were measured to be 1.19–1.70, 1.18, and 1.04 $W \cdot m^{-1} \cdot K^{-1}$, respectively (Mielke et al., 2016). More recently, Heap et al. (2020a) measured the thermal properties (thermal conductivity, thermal diffusivity, and specific heat capacity) of variably porous andesites from Mt Ruapehu (New Zealand) and variably altered basaltic-andesites from Merapi volcano (Indonesia). The thermal conductivity of low-porosity (~0.05) samples from Mt Ruapehu was measured to be between ~1.4 and ~1.6 $W \cdot m^{-1} \cdot K^{-1}$, but decreased to ~0.4 $W \cdot m^{-1} \cdot K^{-1}$ at a porosity of ~0.6 (Heap et al., 2020a). These authors also found that saturation with water increased the bulk specific heat capacity and thermal conductivity, and decreased the thermal diffusivity, relative to the dry state. Thermal property measurements on samples from Merapi volcano suggested that hydrothermal alteration deceases thermal conductivity and thermal diffusivity, and increases specific heat capacity (Heap et al., 2020a).

Despite these laboratory studies, and others, our understanding of the thermal properties of volcanic rocks stands to benefit from new laboratory data. In particular, little is known about the influence of hydrothermal alteration on the thermal properties of volcanic rocks. However, an understanding as to how hydrothermal alteration can influence thermal properties is important. This is because increasing volcanic unrest resulting in an elevated heat flux, which is linked to impending magmatic and phreatic eruptions (Girona et al., 2021), is often associated with a visible increase in alteration (Jessop et al., 2021). Here, we report findings from a

126 laboratory study designed to better understand the influence of hydrothermal alteration on the
127 thermal properties of volcanic rocks, using La Soufrière de Guadeloupe as a case study volcano.
128
129 **2 La Soufrière de Guadeloupe (Eastern Caribbean)**
130 La Soufrière de Guadeloupe (hereafter called La Soufrière) is an active andesitic
131 stratovolcano located on the island of Guadeloupe in the Eastern Caribbean (Figure 1a). There
132 have been six non-magmatic phreatic or hydrothermal eruptions at La Soufrière since 1635 CE,
133 the largest and most-recent eruption of which occurred in 1976–1977 (Komorowski et al.,
134 2005). The 1976–1977 volcanic crisis resulted in the evacuation of ~70,000 people and severe
135 socio-economic consequences for the island of Guadeloupe (Feuillard et al., 1983; Hincks et
136 al., 2014; Komorowski et al., 2005, 2015). Volcanic unrest has been increasing at La Soufrière
137 since 1992, manifest as (1) the formation of new fumaroles and an expansion of the outgassing
138 area on top of the lava dome (Brombach et al., 2000; Komorowski et al., 2005; Villemant et al.,
139 2014; Allard et al., 2014; Moretti et al., 2020), (2) the appearance of high-flow-rate thermal
140 acid sulfate-chloride springs on the slopes and at the base of the dome (Villemant et al., 2005;
141 2014), (3) an increase in the heat output from the dome (Gaudin et al., 2013; Jessop et al., 2021),
142 (4) an increase in seismic activity (hundreds of shallow, low-magnitude earthquakes each
143 month) and the largest felt volcano-tectonic earthquake since 1976–1977 (Moretti et al., 2020),
144 and (5) large flank displacements (Moretti et al., 2020; Heap et al., 2021a).
145 Activity within the shallow hydrothermal system, which has been imaged by a variety
146 of geophysical methods (Nicollin et al., 2006; Brothelande et al., 2014; Bouligand et al., 2016;
147 Rosas-Carbajal et al., 2016), is considered responsible for much of the recent volcanic unrest
148 (Moretti et al., 2020; Heap et al., 2021a). Indeed, La Soufrière has a history of unrest associated
149 with hydrothermal activity. Not only were hydrothermally altered rocks ejected from the vent
150 during the 1976–1977 crisis (Feuillard et al., 1983), but geological evidence have also suggests

that historic partial edifice collapses at La Soufrière were associated with hydrothermal activity, owing to the abundance of hydrothermally altered materials in debris avalanche deposits (Boudon et al., 1987; Komorowski et al., 2005; Le Friant et al., 2006; Salaün et al., 2011; Rosas-Carbajal et al., 2016; Peruzzetto et al., 2019). Because the tropical climate of the island of Guadeloupe (i.e. high yearly precipitation) contributes to dome washout and the shallow hydrothermal regime, La Soufrière represents an ideal natural laboratory to study the influence of hydrothermal alteration on the thermal properties of a nearly fluid-saturated volcanic dome. Further, and importantly, such data are timely due to the link between magmatic and phreatic eruptions and the increase in heat output associated with increased hydrothermal activity at the volcano (Moretti et al., 2020; Jessop et al., 2021; Girona et al., 2021).

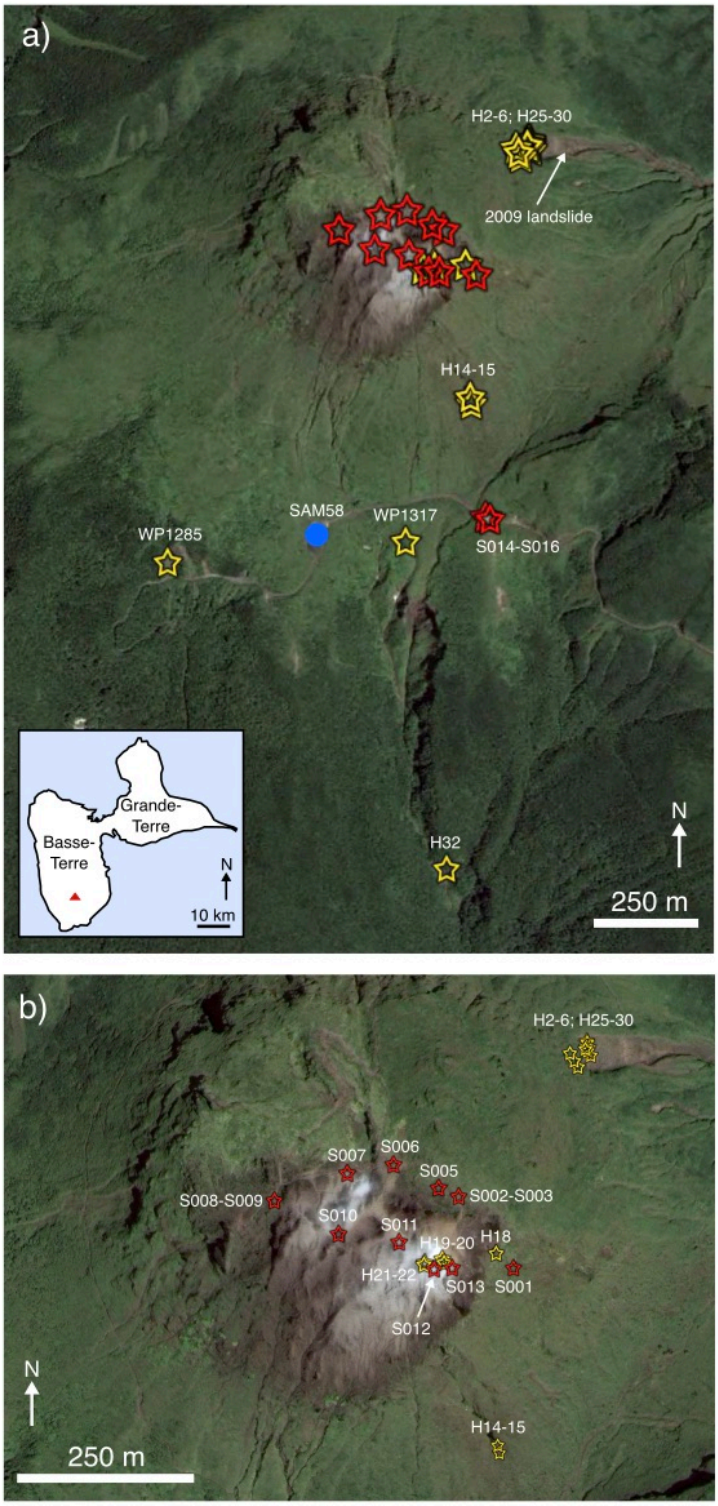

Figure 1. (a) Map of La Soufrière de Guadeloupe (Eastern Caribbean; taken from Google Earth®) showing the sampling locations for the 19 rock blocks of the main sample suite (yellow stars; the "H" series), the 3 rock blocks and 13 bags of unlithified material from the second field campaign (red stars; the "S" series), and the borehole rock sample (blue circle;

SAM58). Inset shows a map of Guadeloupe in which the location of La Soufrière de Guadeloupe is indicated by a red triangle. (b) Zoom of the dome summit area showing the sampling sites on the dome (also taken from Google Earth®).

3 Materials and Methods

Materials (rock blocks and unlithified deposits) were collected over two field campaigns conducted at La Soufrière in 2019. The main sample suite of 19 rock blocks were collected during the first field campaign ("H" series), which were supplemented by 3 rock blocks and 13 bags of unlithified material collected during the second campaign ("S" series). The sampling locations are provided in Figure 1. Our aim was to sample a range of materials from different locations on the volcano that best represent the observed variability in porosity and hydrothermal alteration.

Of the 19 rock blocks from the main sample suite, the "H" series, nine blocks were taken from the collapse scar of the 2009 landslide (H2A, H2B, H3, H4A, H5A, H6, H25, H29, and H30). Five blocks were collected from the dome summit: four blocks were taken from the lava spines of the 1530 CE dome (two blocks from *Cratère Sud Central*, H19 and H20, and two blocks from an adjacent site, H21 and H22), and one block was taken from the *Lacroix Supérieur* outgassing fracture (H18). We also collected blocks from the West wall of the fault *Faille 30 août* (H14 and H15), the collapse scar of the landslide triggered by the 21 November 2004 *Les Saintes* magnitude Mw 6.3 regional earthquake (Feuillet et al., 2011) (WP1285), and adjacent to the *Galion* waterfall (H32). The final block, a volcanic bomb from the 1976–1977 eruption, was taken from the roof of a small disused thermal bathhouse to the South of the dome (WP1317).

Samples in the "S" series were mostly tephra (millimetric granular matter in an argillic matrix). Out of the 16 samples collected, only S005, S008, and S016 were rock blocks. S001

192 was taken from just below the summit plateau to the East of the dome. Notably, this location is
193 upwind of the predominant wind direction and thus the sample was relatively uncontaminated
194 by fumarolic gases. Samples S002–S006 were taken from within the thermally-active zone
195 (called "ZFNN" in Jessop et al., 2021), but from locations mostly unaffected by strong
196 outgassing. S007 was taken directly downwind and from the rim of the *Tarrisan* crater. Samples
197 S008–S011 were taken from various sites downwind of the main outgassing sites, and samples
198 S012 and S013 were collected in proximity to the main outgassing vents. Finally, samples
199 S014–S016 were taken from the base of the volcano, close to a site with low-level, passive
200 degassing and highly-altered soils due to historical high-activity. An additional rock sample
201 was taken from a borehole (SAM58) located at the *Savane à Mulets* carpark on the southwest
202 base of the dome (Figure 1a). This sample was taken from a depth of ~58 m.

203 Multiple cylindrical samples were cored from each of the rock blocks (from the "H" and
204 "S" series) to a diameter of 20 mm, and then cut and precision-ground to a nominal length of
205 40 mm. The samples were washed and then dried in a vacuum-oven at 40 °C for at least 48 h.
206 The connected porosity of each sample was calculated using the bulk sample volume and the
207 skeletal (solid) sample volume measured by a helium pycnometer. The cylindrical samples
208 prepared from each block were then grouped into pairs of similar porosity. For most blocks,
209 three pairs of samples were measured. For certain blocks (H15, H30, SAM58, S005, S008, and
210 S016), which were smaller, only two pairs of samples were measured.

211 The unlithified materials were first sieved to a grain diameter < 2 mm and then dried in
212 a vacuum-oven at 40 °C for at least 48 h. The solid density of each unlithified sample was then
213 measured using the mass and volume, measured by a helium pycnometer, of an aliquot of the
214 oven-dry powder.

215 The thermal conductivity, λ (in units of $W \cdot m^{-1} \cdot K^{-1}$), and thermal diffusivity, D (in units
216 of $mm^2 \cdot s^{-1}$), were measured using a Hot Disk® TPS 500 Thermal Constants Analyser using the

transient plane source method (Gustafsson, 1991; Gustavsson et al., 1994; Harlé et al., 2019; Heap et al., 2020a). The transient plane source method is a periodic method to measure the thermal properties of materials (Hofmeister, 2019). The standard uncertainties for thermal conductivity and thermal diffusivity values using the transient hot-strip method, arising from contact losses and ballistic radiative transfer gains (Hofmeister, 2019), were determined to be 2.6 and 11%, of the measured values respectively (Hammerschmidt and Sabuga, 2000).

Thermal conductivity and thermal diffusivity were measured using a sensor consisting of two 10 μm-thick nickel foil spirals (radius of 3.189 mm) that are encased and insulated by 30 μm-thick kapton (see inset on Figure 2a). For the rock samples, the sensor was sandwiched between two cylindrical samples, of similar porosity, cored from the same block (Figure 2a). The rock samples were held in place using a screw positioned at the top of the sample jig (Figure 2a), which ensured good contact between the sensor and the surface of the samples.

The unlithified samples were measured using a sample holder of known volume supplied by Hot Disk®. Powder was first spooned into the lower part of the sample holder, and the sensor was placed on top of the powder (Figure 2b). The top part of the sample holder was then placed on top of the lower part, and more powder was spooned on top of the sensor (Figure 2c). A plate was then placed on top of the sample assembly, and the entire sample assembly was compacted using a 3.5 kg weight (Figure 2d). The 3.5 kg weight ensured (1) a similar compaction from sample to sample and (2) a good contact between the powder and the sensor.

The temperature adjacent to the sample, measured using a thermocouple, was inputted into the Thermal Constants Analyser prior to starting each measurement. An electrical current of known power and duration was passed through the sensor during the measurement, which also recorded the increase in sample temperature as a function of time. The output power and duration required for a reliable measurement varied from sample to sample and were found using trial-and-error. The output power and test duration were typically 100–200 mW and 5–

10 s, respectively. Four consecutive measurements were performed on each pair of samples (on the four different combinations of sample end-faces) and each powder, and we report herein an average of these four measurements. Each measurement was performed at least five minutes apart to ensure that the sample had cooled back to the ambient temperature. The sensor measured the temperature drift of the sample for 40 seconds prior to each measurement to check whether the sample was in thermal equilibrium. If the sample temperature was not constant during this 40 second period, the data were not considered and the measurement was repeated. Following each set of measurements on the powder samples, the mass of the powder was measured to provide the bulk sample density and, using the solid density of each powder, their total porosities were calculated. The volumetric heat capacity, $\rho_b C_p$ (in units of $J \cdot m^{-3} \cdot K^{-1}$), calculated by the Hot Disk® device, was divided by the independently determined bulk sample density, ρ_b, to provide the bulk sample specific heat capacity, C_p (in units of $J \cdot kg^{-1} \cdot K^{-1}$). All measurements were conducted in a far-field environment that was at ambient laboratory temperature and pressure.

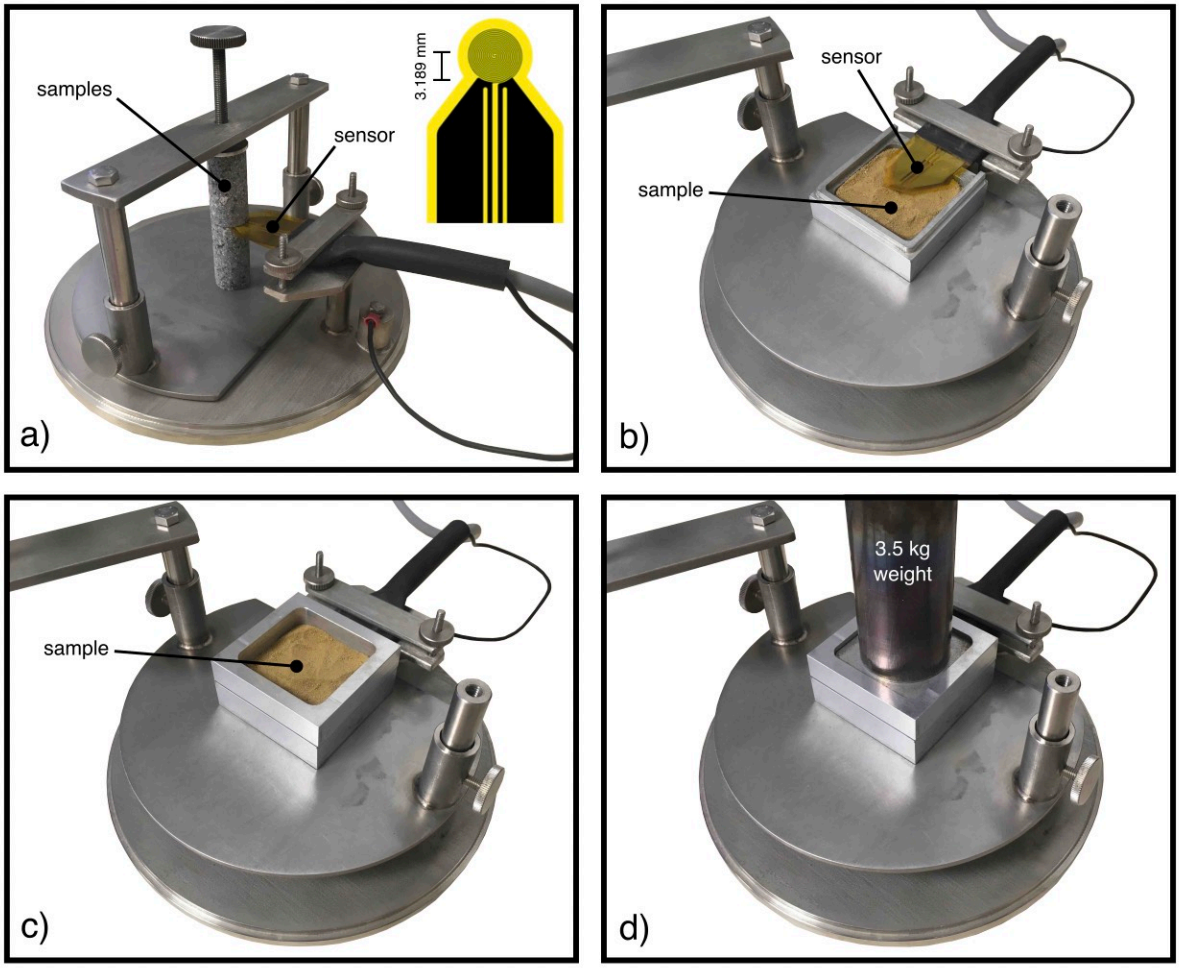

Figure 2. (a) Photograph of the experimental setup for the rock-rock measurements. Insets show the sensor used, consisting of two 10 μm-thick nickel foil spirals (radius of 3.189 mm) that are encased and insulated by 30 μm-thick kapton (used for all measurements). The screw on the top of the setup ensures a good contact between the sensor and the samples. Panels (b), (c), and (d) are photographs that show the procedure for measuring a powder sample. (b) The powder was first spooned into the lower part of the holder, underneath the sensor. (c) The upper part of the holder was placed onto the lower part and powder was spooned over the sensor. (d) The top of the holder (a flat piece) was placed on top of the powder and a 3.5 kg weight was placed on top of the setup to ensure reproduceable compaction and a good contact between the sensor and the powder.

Polished thin sections were prepared from offcuts of the main sample suite (the "H" series) for microstructural analysis using a Tescan Vega 2 XMU scanning electron microscope (SEM). The mineral contents of 17 of the 19 blocks from the "H" series, collected during the first field campaign, were quantified using X-ray powder diffraction (XRPD) in Heap et al. (2021a). We provide here the mineral contents of the two remaining samples from this sample suite (samples H30 and H32), using the same technique described in Heap et al. (2021a). To do so, powdered offcuts of the core material were ground for 8 min with 10 ml of isopropyl alcohol in a McCrone Micronising Mill using ZrO_2 cylinder elements. The XRPD analyses were performed on side-loaded powder mounts using a Bruker D8 Advance Eco X-ray diffractometer (CuKα, 40 kV, 25 mA, 2–75° 2θ, 0.01° step size, 15 mm irradiated length, 2.5° primary and secondary sollers, and a LynxEye XE-T detector). The phases in the whole rock powders were then quantified using the Rietveld program BGMN (Bergmann et al., 1998) and the Profex graphical user interface (Döbelin and Kleeberg, 2015). To identify clay minerals, < 2 μm fractions were separated by gravitational settling, and oriented mounts were X-rayed in an air-dried state, an ethylene-glycolated state, and following exposure to 550 °C. Selected mineral phases were additionally identified by micro-Raman spectroscopy using a Horiba Jobin Yvon XploRA PLUS confocal Raman microscope. The spectrometer was equipped with a frequency-double Nd:YAG laser (532 nm, with a maximum power of 22.5 mW) and an Olympus LMPLFLN 100× long-working-distance objective with a numerical aperture of 0.9.

4 Results

4.1 Microstructure, mineralogy, and alteration

The mineral contents for each of the 19 rock blocks from the main sample suite ("H" series) are available in Table 1 (data for all but samples H30 and H32 were presented in Heap et al., 2021a). All of the andesite blocks are characterised by a porphyritic texture comprising

phenocrysts (often a few hundred microns long, but occasionally as large as 1–2 mm) of dominantly plagioclase and pyroxene (orthopyroxene and clinopyroxene) within a crystallised groundmass (Figures 3 and 4; Heap et al., 2021a). Microcracks and pores (with a diameter ranging from a couple of tens of microns to almost 1 mm) are present in all of the samples (Figures 3 and 4; Heap et al., 2021a).

All of the samples also contain variable quantities of secondary minerals, including kaolinite, alunite or natro-alunite, silica polymorphs (quartz, cristobalite, tridymite, and opal-A), hematite, pyrite, gypsum, and talc (secondary minerals are indicated by asterisks in Table 1). The most abundant secondary minerals are kaolinite, natro-alunite, and cristobalite (Table 1). Kaolinite is present as a replacement mineral in altered plagioclases and as a microcrack- and pore-filling precipitate, and natro-alunite and cristobalite are present as microcrack- and pore-filling precipitates (Figures 3 and 4). The observed secondary mineral assemblage corresponds to intermediate to advanced argillic alteration (Heap et al., 2021a).

Based on the results of the XRPD, each of the 19 rock blocks from the "H" series are assigned a value of alteration—the weight percentage of secondary minerals in the block—which ranges from 6 wt.% (sample H32) up to 85.4 wt.% (sample H30) (Table 2).

Mineral	H2A	H2B	H3	H4A	H5A	H6	H14	H15	H18	H19	H20	H21	H22	H25	H29	H30	H32	WP1285	WP1317
Plagioclase	56.7	12.3	46.6	23.3	41.3	30.0	60.7	22.5	61.2	22.0	28.7	24.2	59.5	38.7	62.4	8.9	64.4	64.7	61.6
Clinopyroxene	8.7	3.4	5.6	4.9	5.2	6.4	6.3	7.3	8.4	5.0	8.9	12.4	8.9	5.3	7.8	2.5	9.5	5.2	5.9
Orthopyroxene	10.8	9.5	11.8	11.8	11.1	10.8	8.6	9.2	12.2	10.2	15.0	19.3	13.6	10.2	11.2	3.3	15.1	13.2	15.6
(Ti-) Magnetite	0.7	-	0.8	-	-	-	0.8	-	2.9	-	2.4	3.1	0.8	-	2.7		4.9	3.5	0.7
Quartz*	1.0	0.5	0.6	0.6	0.5	0.5	1.7	0.7	0.7	1.7	0.3	0.2	0.6	0.3	0.4	0.9	0.3	0.2	0.7
Cristobalite*	11.3	12.8	10.6	11.8	13.0	11.1	13.5	10.2	11.7	9.5	11.4	11.7	10.6	9.8	12.4	9	5.7	-	-
Tridymite*	-	-	-	-	-	-	-	0.7	-	-	-	-	-	-	-			13.2	13.2
Hematite*	-	-	-	-	-	-	3.4	-	2.8	2.4	-	-	-	-	3.1	4.3		-	-
Pyrite*	3.5	-	3.8	2.3	-	-	-	-	-	-	-	0.4	3.1	0.6	-			-	-
Alunite*	-	-	-	-	-	-	-	-	-	-	-	-	-	-	-			-	2.4
Na-Alunite*	1.4	1.6	2.8	1.3	5.4	5.1	5.1	15.0	-	14.2	0.5	0.5	-	9.8	-	25.6		-	-
Gypsum*	-	-	-	0.7	-	-	-	-	-	-	0.8	1.2	-	-	-			-	-
Kaolinite*	6	59.7	17.4	43.3	23.5	36.0	< 1	34.3	-	2.0	2.0	2.0	< 1	25.3	-	35.6		-	-
Talc*	-	-	-	-	-	-			-	-	-	-	2.9	-	-			-	-
Opal-A*	-	-	-	-	-	-			33.0	30.0	25.0	-	-	-	10.0	10		-	-

312 **Table 1.** Mineral contents, measured by X-ray powder diffraction, of the 19 rock blocks from
313 the main sample suite ("H" series). Values in wt.%. Asterisk denotes a secondary mineral (i.e.
314 alteration mineral). All data, except those for H30 and H32, were taken from Heap et al.
315 (2021a).
316

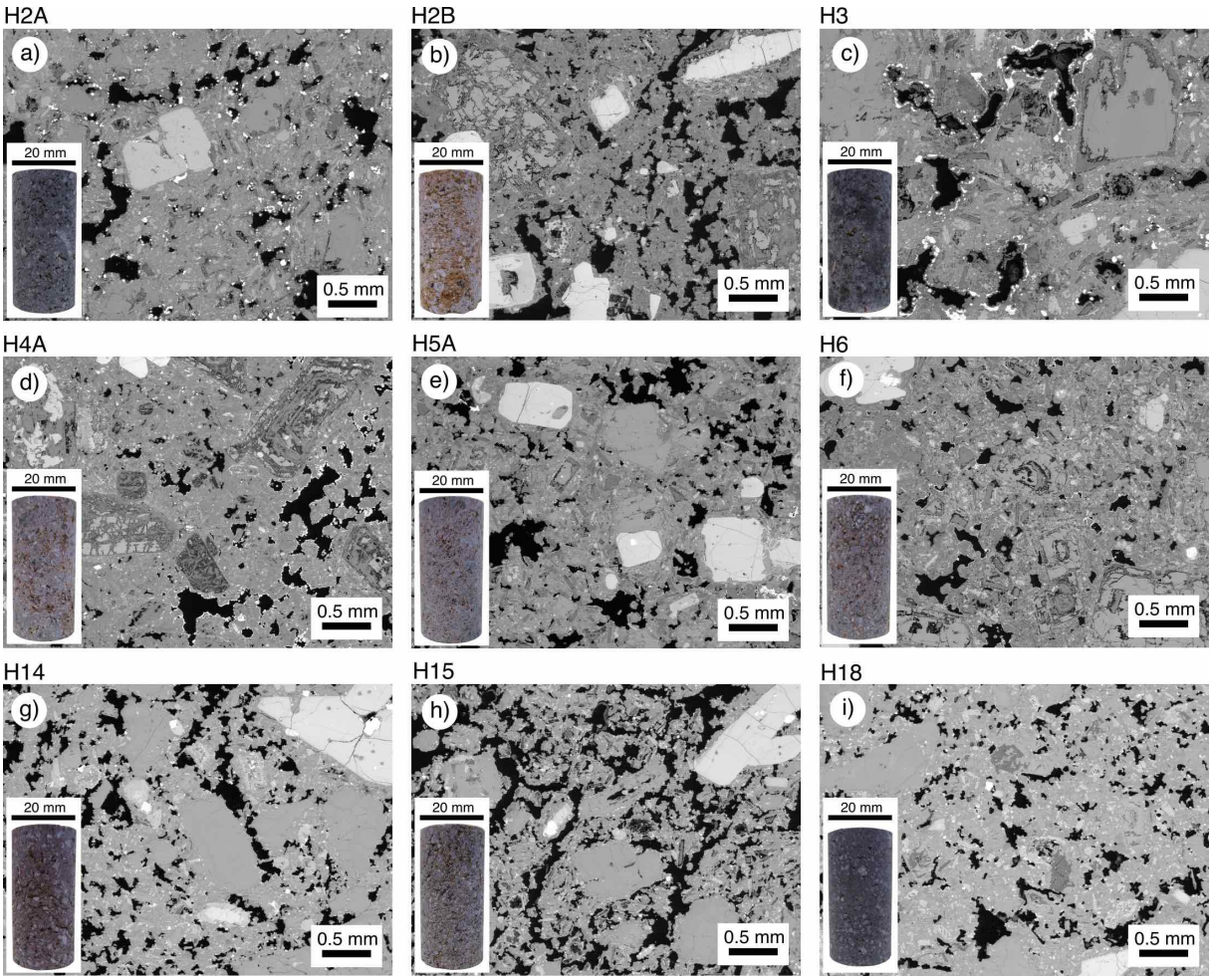

317
318 **Figure 3.** Backscattered scanning electron microscope images of andesites from La Soufrière
319 de Guadeloupe (Eastern Caribbean). Insets show a photograph of 20 mm-diameter sample
320 prepared from the block. (a) H2A. (b) H2B. (c) H3. (d) H4A. (e) H5A. (f) H6. (g) H14. (h)
321 H15. (i) H18.
322

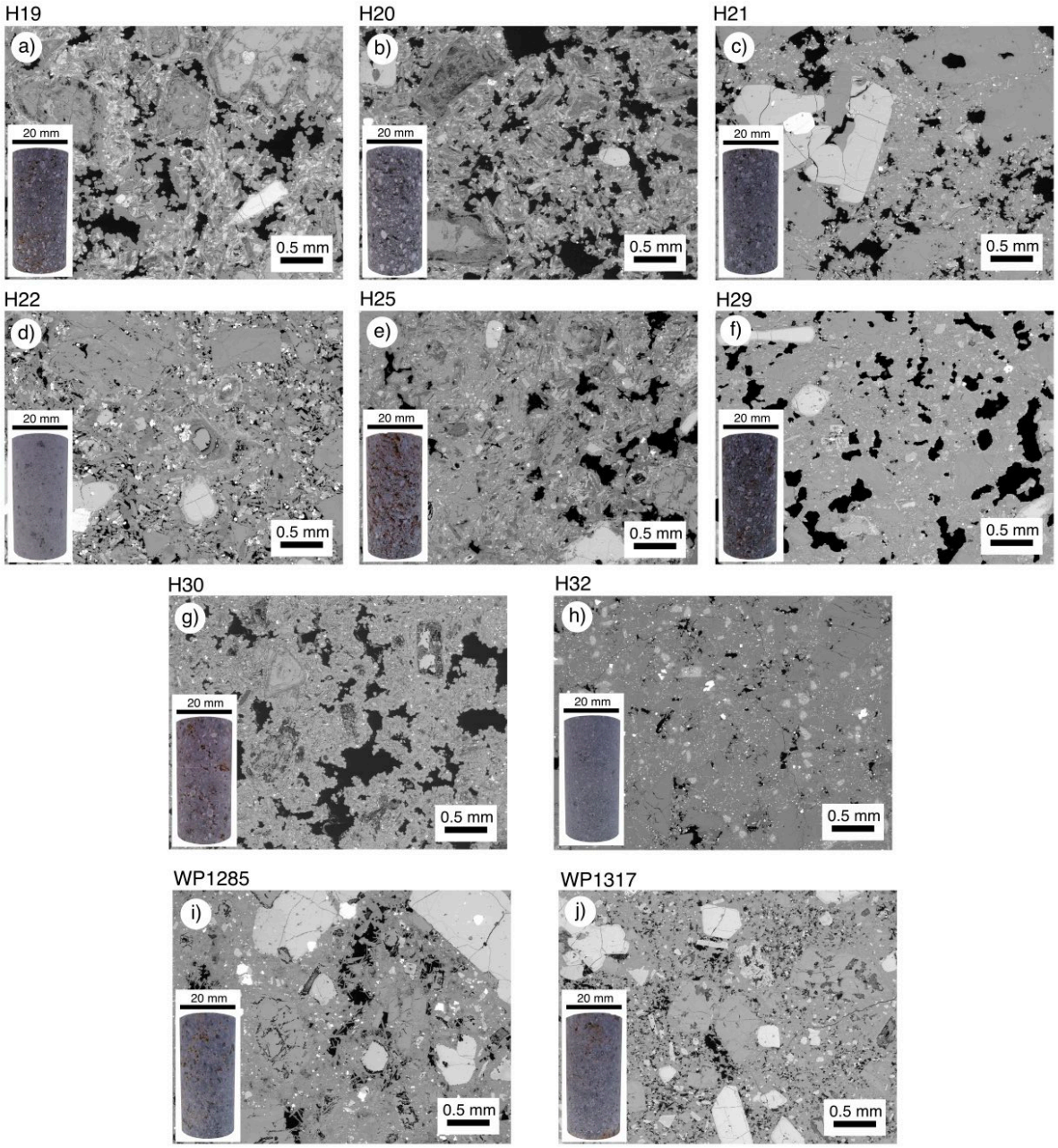

323

324 **Figure 4.** Backscattered scanning electron microscope images of andesites from La Soufrière
325 de Guadeloupe (Eastern Caribbean). Insets show a photograph of 20 mm-diameter sample
326 prepared from the block. (a) H19. (b) H20. (c) H21. (d) H22. (e) H25. (f) H29. (g) H30. (h)
327 H32. (i) WP1285. (j) WP1317.

328

329 4.2 Thermal properties

Thermal conductivity, thermal diffusivity, and specific heat capacity for all the samples (rocks and powders) are plotted as a function of porosity in Figure 5 (data available in Table 2). If we consider both types of sample (rocks and powders), we find that thermal conductivity and thermal diffusivity decrease as a function of porosity, and that specific heat capacity does not change systematically as a function of porosity (Figure 5). The trend with increasing porosity is much more evident in the thermal conductivity data (Figure 5a) than in the thermal diffusivity data (Figure 5b).

The porosity of the rock samples varies from 0.04 to 0.44, and the porosity of the powders during the measurements, compacted using a 1 kg weight, varies between 0.51 and 0.61. For the rock samples, thermal conductivity decreases from ~1.6 $W \cdot m^{-1} \cdot K^{-1}$ at a porosity of ~0.04 to ~0.5 $W \cdot m^{-1} \cdot K^{-1}$ at a porosity of ~0.4 (Figure 5a). The thermal conductivity of the powder samples is ~0.2 $W \cdot m^{-1} \cdot K^{-1}$ for all samples (Figure 5a). The thermal diffusivity of the rock samples generally decreases from ~0.9 to ~0.3 $mm^2 \cdot s^{-1}$ as porosity increases, and the thermal diffusivity of the powder samples is ~0.22 $mm^2 \cdot s^{-1}$ for all samples (Figure 5b). Excluding a few outliers, the specific heat capacity is ~0.8 $kJ \cdot kg^{-1} \cdot K^{-1}$ for all samples (rocks and powders), regardless of their porosity (Figure 5c).

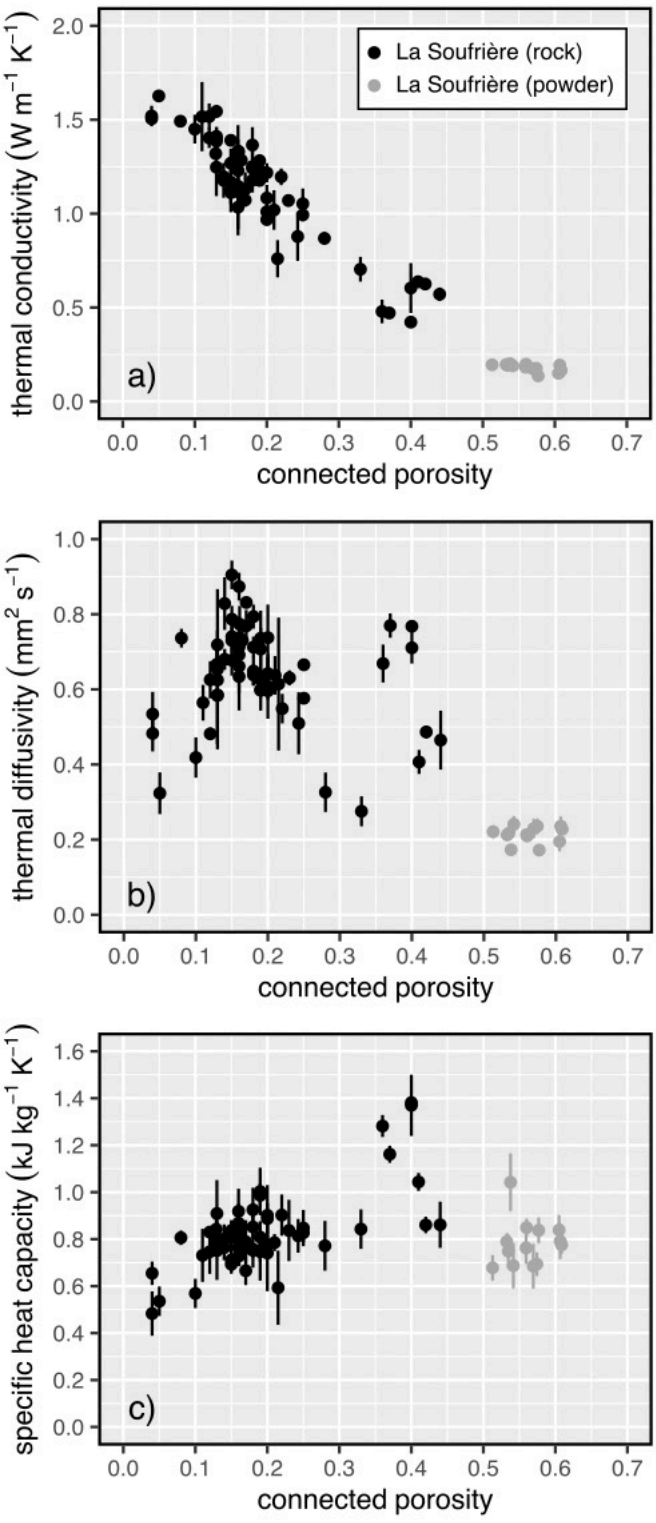

347

348 **Figure 5.** Thermal conductivity, thermal diffusivity, and specific heat capacity as a function
349 of connected porosity for the rocks (black symbols) and unlithified materials (powders; grey
350 symbols) from La Soufrière de Guadeloupe (Eastern Caribbean).

351

sample number	sample type	connected porosity	weight percentage of secondary minerals	thermal conductivity ($W \cdot m^{-1} \cdot K^{-1}$)	thermal diffusivity ($mm^2 \cdot s^{-1}$)	specific heat capacity ($kJ \cdot kg^{-1} \cdot K^{-1}$)
H2A	rock	0.18	23.2	1.37 ± 0.10	0.79 ± 0.03	0.75 ± 0.03
H2A	rock	0.19	23.2	1.23 ± 0.08	0.74 ± 0.07	0.75 ± 0.13
H2A	rock	0.20	23.2	1.01 ± 0.04	0.60 ± 0.02	0.77 ± 0.04
H2B	rock	0.42	74.6	0.63 ± 0.02	0.49 ± 0.02	0.86 ± 0.04
H2B	rock	0.44	74.6	0.57 ± 0.04	0.46 ± 0.08	0.86 ± 0.10
H2B	rock	0.41	74.6	0.64 ± 0.03	0.41 ± 0.03	1.04 ± 0.04
H3	rock	0.19	35.2	1.28 ± 0.03	0.62 ± 0.04	0.99 ± 0.05
H3	rock	0.16	35.2	1.33 ± 0.06	0.69 ± 0.10	0.87 ± 0.15
H3	rock	0.15	35.2	1.39 ± 0.03	0.73 ± 0.01	0.84 ± 0.02
H4A	rock	0.23	60.0	1.07 ± 0.03	0.63 ± 0.02	0.84 ± 0.13
H4A	rock	0.25	60.0	0.99 ± 0.03	0.67 ± 0.01	0.85 ± 0.08
H4A	rock	0.20	60.0	1.08 ± 0.07	0.64 ± 0.04	0.89 ± 0.07
H5A	rock	0.16	42.4	1.28 ± 0.06	0.66 ± 0.03	0.80 ± 0.03
H5A	rock	0.18	42.4	1.25 ± 0.02	0.64 ± 0.03	0.85 ± 0.05
H5A	rock	0.15	42.4	1.27 ± 0.08	0.68 ± 0.04	0.82 ± 0.05
H6	rock	0.18	52.7	1.18 ± 0.02	0.65 ± 0.04	0.93 ± 0.09
H6	rock	0.19	52.7	1.18 ± 0.02	0.60 ± 0.06	1.00 ± 0.10
H6	rock	0.16	52.7	1.23 ± 0.02	0.71 ± 0.05	0.82 ± 0.08
H14	rock	0.19	23.7	1.20 ± 0.03	0.71 ± 0.06	0.75 ± 0.04
H14	rock	0.20	23.7	1.22 ± 0.05	0.61 ± 0.09	0.90 ± 0.13
H14	rock	0.18	23.7	1.24 ± 0.13	0.71 ± 0.03	0.76 ± 0.08
H15	rock	0.28	60.9	0.87 ± 0.03	0.33 ± 0.05	0.77 ± 0.11
H15	rock	0.33	60.9	0.70 ± 0.07	0.28 ± 0.04	0.84 ± 0.08
H18	rock	0.13	15.2	1.39 ± 0.08	0.59 ± 0.02	0.80 ± 0.05
H18	rock	0.13	15.2	1.41 ± 0.05	0.65 ± 0.21	0.79 ± 0.05
H18	rock	0.12	15.2	1.40 ± 0.05	0.48 ± 0.02	0.83 ± 0.02
H19	rock	0.15	62.8	1.13 ± 0.04	0.74 ± 0.04	0.69 ± 0.03
H19	rock	0.17	62.8	1.07 ± 0.04	0.77 ± 0.04	0.67 ± 0.06
H19	rock	0.20	62.8	0.97 ± 0.03	0.74 ± 0.09	0.74 ± 0.16
H20	rock	0.37	45.0	0.47 ± 0.03	0.77 ± 0.03	1.16 ± 0.04
H20	rock	0.36	45.0	0.48 ± 0.06	0.67 ± 0.05	1.28 ± 0.05
H20	rock	0.40	45.0	0.42 ± 0.02	0.71 ± 0.04	1.37 ± 0.13
H21	rock	0.15	41.0	1.17 ± 0.12	0.90 ± 0.04	0.71 ± 0.06
H21	rock	0.17	41.0	1.13 ± 0.09	0.83 ± 0.01	0.79 ± 0.09
H21	rock	0.16	41.0	1.12 ± 0.20	0.87 ± 0.04	0.77 ± 0.04
H22	rock	0.12	17.2	1.52 ± 0.07	0.63 ± 0.05	0.75 ± 0.09
H22	rock	0.11	17.2	1.52 ± 0.18	0.56 ± 0.05	0.73 ± 0.11
H22	rock	0.13	17.2	1.54 ± 0.03	0.62 ± 0.02	0.77 ± 0.03
H25	rock	0.16	45.8	1.15 ± 0.07	0.63 ± 0.09	0.85 ± 0.10
H25	rock	0.21	45.8	1.02 ± 0.11	0.64 ± 0.05	0.79 ± 0.04
H25	rock	0.14	45.8	1.20 ± 0.03	0.68 ± 0.03	0.76 ± 0.05
H29	rock	0.22	25.9	1.20 ± 0.04	0.55 ± 0.04	0.90 ± 0.09
H29	rock	0.25	25.9	1.05 ± 0.08	0.58 ± 0.02	0.83 ± 0.04
H29	rock	0.19	25.9	1.20 ± 0.04	0.60 ± 0.02	0.81 ± 0.06

H30	rock	0.16	85.4	1.30 ± 0.17	0.74 ± 0.01	0.92 ± 0.01
H30	rock	0.40	85.4	0.60 ± 0.13	0.77 ± 0.01	1.38 ± 0.02
H32	rock	0.04	6.0	1.52 ± 0.05	0.48 ± 0.05	0.65 ± 0.05
H32	rock	0.04	6.0	1.51 ± 0.01	0.53 ± 0.06	0.48 ± 0.09
H32	rock	0.05	6.0	1.63 ± 0.01	0.32 ± 0.06	0.54 ± 0.06
WP1317	rock	0.16	16.3	1.03 ± 0.15	0.73 ± 0.03	0.85 ± 0.05
WP1317	rock	0.15	16.3	1.11 ± 0.10	0.79 ± 0.04	0.81 ± 0.07
WP1317	rock	0.14	16.3	1.18 ± 0.09	0.83 ± 0.07	0.80 ± 0.06
WP1285	rock	0.13	13.4	1.40 ± 0.02	0.72 ± 0.04	0.75 ± 0.12
WP1285	rock	0.10	13.4	1.45 ± 0.08	0.42 ± 0.05	0.57 ± 0.06
WP1285	rock	0.08	13.4	1.49 ± 0.01	0.74 ± 0.02	0.81 ± 0.03
SAM58	rock	0.14	-	1.18 ± 0.02	0.66 ± 0.03	0.75 ± 0.05
SAM58	rock	0.14	-	1.21 ± 0.05	0.65 ± 0.03	0.78 ± 0.04
S005	rock	0.22	-	0.76 ± 0.10	0.61 ± 0.18	0.59 ± 0.16
S005	rock	0.24	-	0.88 ± 0.13	0.51 ± 0.08	0.81 ± 0.07
S008	rock	0.17	-	1.28 ± 0.04	0.73 ± 0.03	0.75 ± 0.02
S008	rock	0.16	-	1.33 ± 0.02	0.77 ± 0.05	0.73 ± 0.04
S016	rock	0.13	-	1.32 ± 0.03	0.67 ± 0.05	0.84 ± 0.06
S016	rock	0.13	-	1.25 ± 0.15	0.58 ± 0.13	0.91 ± 0.14
S001	powder	0.61	-	0.19 ± 0.00	0.24 ± 0.02	0.79 ± 0.08
S002	powder	0.56	-	0.20 ± 0.01	0.21 ± 0.01	0.85 ± 0.04
S003	powder	0.53	-	0.20 ± 0.01	0.21 ± 0.00	0.79 ± 0.03
S004	powder	0.61	-	0.15 ± 0.01	0.19 ± 0.03	0.84 ± 0.06
S006	powder	0.57	-	0.18 ± 0.01	0.23 ± 0.03	0.68 ± 0.09
S007	powder	0.56	-	0.18 ± 0.01	0.21 ± 0.02	0.76 ± 0.07
S009	powder	0.51	-	0.20 ± 0.01	0.22 ± 0.02	0.68 ± 0.05
S010	powder	0.54	-	0.19 ± 0.01	0.22 ± 0.01	0.75 ± 0.07
S011	powder	0.57	-	0.18 ± 0.00	0.24 ± 0.02	0.69 ± 0.05
S012	powder	0.61	-	0.17 ± 0.01	0.23 ± 0.01	0.78 ± 0.04
S013	powder	0.54	-	0.19 ± 0.01	0.24 ± 0.02	0.69 ± 0.10
S014	powder	0.58	-	0.14 ± 0.00	0.17 ± 0.01	0.84 ± 0.05
S015	powder	0.54	-	0.20 ± 0.02	0.17 ± 0.01	1.04 ± 0.12

Table 2. Connected porosity, weight percentage of secondary minerals, thermal conductivity, thermal diffusivity, and specific heat capacity for the samples from La Soufrière de Guadeloupe (Eastern Caribbean) measured for this study. The standard deviations provided relate to measurement precision (calculated using the four measurements). The standard uncertainty for values of thermal conductivity and thermal diffusivity using the transient hot-strip method has been determined to be 2.6 and 11%, respectively (Hammerschmidt and Sabuga, 2000).

360

volcano	rock type	connected porosity	weight percentage of secondary minerals	thermal conductivity ($W \cdot m^{-1} \cdot K^{-1}$)	thermal diffusivity ($mm^2 \cdot s^{-1}$)	specific heat capacity ($kJ \cdot kg^{-1} \cdot K^{-1}$)
Chaos Crags	rhyodacite	0.153	6.4	1.14 ± 0.03	0.65 ± 0.02	0.78 ± 0.02
Chaos Crags	rhyodacite	0.139	14.6	1.29 ± 0.03	0.73 ± 0.07	0.78 ± 0.08
Chaos Crags	rhyodacite	0.125	14.6	1.52 ± 0.26	0.84 ± 0.09	0.77 ± 0.07
Chaos Crags	rhyodacite	0.138	14.6	1.40 ± 0.24	0.94 ± 0.06	0.66 ± 0.15
Chaos Crags	rhyodacite	0.076	16.5	1.66 ± 0.09	0.89 ± 0.07	0.77 ± 0.02
Chaos Crags	rhyodacite	0.142	16.5	1.51 ± 0.28	0.90 ± 0.13	0.72 ± 0.05
Chaos Crags	rhyodacite	0.115	16.5	1.44 ± 0.17	0.78 ± 0.11	0.78 ± 0.03
Merapi	basaltic-andesite	0.080	7.5	1.43 ± 0.02	0.70 ± 0.04	0.79 ± 0.03
Merapi	basaltic-andesite	0.084	7.5	1.37 ± 0.03	0.73 ± 0.03	0.74 ± 0.02
Merapi	basaltic-andesite	0.077	7.5	1.48 ± 0.02	0.73 ± 0.04	0.79 ± 0.04
Merapi	basaltic-andesite	0.079	29.0	1.20 ± 0.02	0.57 ± 0.02	0.86 ± 0.04
Merapi	basaltic-andesite	0.080	29.0	1.23 ± 0.05	0.57 ± 0.03	0.87 ± 0.02
Merapi	basaltic-andesite	0.083	29.0	1.28 ± 0.01	0.53 ± 0.02	0.98 ± 0.03
Merapi	basaltic-andesite	0.154	45.0	1.06 ± 0.07	0.51 ± 0.03	0.90 ± 0.04
Merapi	basaltic-andesite	0.182	45.0	0.90 ± 0.06	0.51 ± 0.03	0.81 ± 0.01
Merapi	basaltic-andesite	0.144	45.0	1.07 ± 0.05	0.53 ± 0.01	0.91 ± 0.06
Merapi	basaltic-andesite	0.155	45.0	1.04 ± 0.01	0.52 ± 0.02	0.88 ± 0.04
Merapi	basaltic-andesite	0.160	45.0	0.97 ± 0.08	0.54 ± 0.03	0.81 ± 0.06
Merapi	basaltic-andesite	0.162	45.0	0.97 ± 0.01	0.66 ± 0.21	0.73 ± 0.23
Merapi	basaltic-andesite	0.182	45.0	0.94 ± 0.00	0.43 ± 0.00	0.99 ± 0.00
Merapi	basaltic-andesite	0.215	62.0	0.78 ± 0.08	0.60 ± 0.09	0.66 ± 0.18
Merapi	basaltic-andesite	0.233	62.0	0.80 ± 0.04	0.51 ± 0.09	0.79 ± 0.10
Merapi	basaltic-andesite	0.220	62.0	0.86 ± 0.07	0.51 ± 0.04	0.82 ± 0.02
Merapi	basaltic-andesite	0.188	62.0	0.86 ± 0.06	0.50 ± 0.03	0.82 ± 0.02
Merapi	basaltic-andesite	0.163	62.0	0.88 ± 0.01	0.55 ± 0.04	0.75 ± 0.06
Merapi	basaltic-andesite	0.242	62.0	0.79 ± 0.05	0.46 ± 0.00	0.86 ± 0.05
Merapi	basaltic-andesite	0.263	62.0	0.79 ± 0.01	0.47 ± 0.04	0.88 ± 0.07
Merapi	basaltic-andesite	0.168	62.0	0.85 ± 0.03	0.44 ± 0.09	0.92 ± 0.19
Merapi	basaltic-andesite	0.231	32.5	0.75 ± 0.06	0.45 ± 0.06	0.80 ± 0.11
Merapi	basaltic-andesite	0.236	32.5	0.76 ± 0.05	0.51 ± 0.02	0.70 ± 0.07
Merapi	basaltic-andesite	0.262	32.5	0.76 ± 0.04	0.55 ± 0.11	0.70 ± 0.11
Merapi	basaltic-andesite	0.256	32.5	0.75 ± 0.05	0.47 ± 0.05	0.78 ± 0.06
Ruapehu	andesite	0.021	-	1.54 ± 0.02	0.70 ± 0.02	0.80 ± 0.03
Ruapehu	andesite	0.040	-	1.62 ± 0.02	0.77 ± 0.02	0.78 ± 0.01
Ruapehu	andesite	0.024	-	1.47 ± 0.06	0.77 ± 0.07	0.72 ± 0.10
Ruapehu	andesite	0.036	-	1.46 ± 0.05	0.75 ± 0.01	0.73 ± 0.02
Ruapehu	andesite	0.042	-	1.53 ± 0.01	0.76 ± 0.03	0.74 ± 0.04
Ruapehu	andesite	0.047	-	1.51 ± 0.05	0.72 ± 0.05	0.79 ± 0.09
Ruapehu	andesite	0.038	-	1.45 ± 0.03	0.70 ± 0.03	0.77 ± 0.05
Ruapehu	andesite	0.036	-	1.50 ± 0.00	0.72 ± 0.01	0.78 ± 0.01
Ruapehu	andesite	0.024	-	1.48 ± 0.02	0.71 ± 0.02	0.77 ± 0.03
Ruapehu	andesite	0.027	-	1.46 ± 0.03	0.68 ± 0.01	0.79 ± 0.00
Ruapehu	andesite	0.048	-	1.39 ± 0.01	0.83 ± 0.06	0.64 ± 0.04
Ruapehu	andesite	0.042	-	1.41 ± 0.00	0.66 ± 0.00	0.80 ± 0.00
Ruapehu	andesite	0.184	-	1.06 ± 0.01	0.65 ± 0.04	0.73 ± 0.05
Ruapehu	andesite	0.205	-	1.00 ± 0.05	0.58 ± 0.05	0.79 ± 0.11
Ruapehu	andesite	0.098	-	1.26 ± 0.01	0.70 ± 0.04	0.72 ± 0.04
Ruapehu	andesite	0.118	-	1.22 ± 0.06	0.65 ± 0.05	0.77 ± 0.10

Ruapehu	andesite	0.153	-	1.16 ± 0.05	0.66 ± 0.08	0.75 ± 0.06
Ruapehu	andesite	0.140	-	1.23 ± 0.05	0.71 ± 0.06	0.73 ± 0.08
Ruapehu	andesite	0.149	-	1.14 ± 0.04	0.65 ± 0.02	0.73 ± 0.05
Ruapehu	andesite	0.167	-	1.08 ± 0.09	0.72 ± 0.09	0.65 ± 0.03
Ruapehu	andesite	0.129	-	1.21 ± 0.04	0.59 ± 0.01	0.86 ± 0.04
Ruapehu	andesite	0.151	-	1.13 ± 0.05	0.60 ± 0.06	0.80 ± 0.05
Ruapehu	andesite	0.204	-	1.01 ± 0.05	0.61 ± 0.03	0.75 ± 0.00
Ruapehu	andesite	0.182	-	1.09 ± 0.02	0.62 ± 0.05	0.78 ± 0.05
Ruapehu	andesite	0.308	-	0.81 ± 0.00	0.64 ± 0.03	0.66 ± 0.03
Ruapehu	andesite	0.320	-	0.84 ± 0.00	0.75 ± 0.11	0.61 ± 0.10
Ruapehu	andesite	0.345	-	0.81 ± 0.04	0.52 ± 0.05	0.85 ± 0.05
Ruapehu	andesite	0.348	-	0.81 ± 0.06	0.59 ± 0.02	0.76 ± 0.05
Ruapehu	andesite	0.333	-	0.79 ± 0.05	0.53 ± 0.06	0.81 ± 0.07
Ruapehu	andesite	0.382	-	0.72 ± 0.04	0.63 ± 0.09	0.68 ± 0.14
Ruapehu	andesite	0.602	-	0.43 ± 0.03	0.51 ± 0.04	0.79 ± 0.02
Ruapehu	andesite	0.628	-	0.38 ± 0.03	0.55 ± 0.08	0.71 ± 0.16

Table 3. Connected porosity, weight percentage of secondary minerals, thermal conductivity, thermal diffusivity, and specific heat capacity for the samples from Chaos Crags (USA; data unique to this study), Merapi volcano (Indonesia; data from Heap et al., 2020a), and Ruapehu (New Zealand; data from Heap et al, 2020a). All of the samples listed are rock samples. Alteration (percentage of secondary minerals) of the samples from Merapi volcano was not reported in Heap et al. (2020a). XRPD data are not available for the samples from Ruapehu and so alteration values are not reported. The standard deviations provided relate to measurement precision (calculated using the four measurements). The standard uncertainty for values of thermal conductivity and thermal diffusivity using the transient hot-strip method has been determined to be 2.6 and 11%, respectively (Hammerschmidt and Sabuga, 2000).

5 Discussion

5.1 The influence of porosity on thermal properties

To better understand the influence of porosity on the thermal properties of volcanic rocks, we compare our new data for rocks and powders La Soufrière (Table 2) with published data from Heap et al. (2020a) for rocks from Ruapehu and Merapi volcano (Table 3) and new data for variably-altered rhyodacites from Chaos Crags (Lassen Volcanic National Park,

California, USA) (Table 3). The blocks from Ruapehu are variably porous (from <0.05 to ~0.6) and relatively unaltered porphyritic andesites that contain large phenocrysts of plagioclase and pyroxene within a glassy microlite-rich groundmass (Heap and Kennedy, 2016; Heap et al., 2020a). The blocks from Merapi volcano are variably altered basaltic-andesites with porphyritic texture comprising phenocrysts of dominantly plagioclase and pyroxene within a crystallised groundmass (Heap et al., 2019, 2020a). The alteration phases present are similar to those found in the blocks from La Soufrière, and include natro-alunite, alunite, quartz, hematite, cristobalite, gypsum, and unclassified amorphous phases (Heap et al., 2019, 2020a). The alteration of the blocks from Merapi volcano—the percentage of secondary minerals in the block—ranges from 7.5 wt.% up to 62 wt.% (Table 3). The blocks from Chaos Crags, described in Ryan et al. (2020) and Heap et al. (2021b), are porphyritic rhyodacites containing phenocrysts of dominantly plagioclase, K-feldspar, and quartz within a crystallised groundmass. Secondary minerals include cristobalite, hematite, smectite, and kaolinite (Heap et al., 2021b). The alteration of the rhyodacite blocks from Chaos Crags ranges from 6.4 wt.% up to 16.5 wt.% (Table 3). The thermal properties of cylindrical samples prepared from these blocks (Ruapehu, Merapi volcano, and Chaos Crags) were measured using the same Hot Disk® Thermal Constants Analyser used to measure the samples from La Soufrière, as described above, adding confidence to direct data comparisons.

The effective thermal conductivity, $\lambda(\phi)$, can be determined using the Maxwell result for conduction in a porous medium,

$$\frac{\lambda(\phi)}{\lambda_0} = \frac{(1-\phi)(1-r) + r\beta\phi}{(1-\phi)(1-r) + \beta\phi}, (1)$$

where ϕ is the total porosity, $r = \lambda_f/\lambda_0$ (where λ_f and λ_0 and are the thermal conductivities of the pore-filling fluid and the rock groundmass, respectively; Zimmerman, 1989). We assume

spherical pores, and so $\beta = 3\,(1-r)/(2+r)$ (Zimmerman, 1989). The Maxwell model is a dilute approximation and so assumes no interaction between the spherical pores. Because our thermal conductivity data are for dry materials, we assume a pore fluid thermal conductivity, λ_f, of 0 $W \cdot m^{-1} \cdot K^{-1}$ (i.e. we assume that the conduction of the porosity-filling air is negligible). The Maxwell model for the effect of pores (or any inclusion) on the thermal properties of a medium (Equation (1)) is a dilute approximation for spherical pores or inclusions. By contrast, powders are the effective geometric inverse of spherical pores of gas in a continuum matrix, and are instead discrete (sub-angular or sub-spherical) particles in a continuum gas. Therefore, not only does the Maxwell model (Equation (1)) not apply, but it also is reasonable to expect that the functional form of the appropriate model for powders is different. This is explicitly documented in Torquato and Haslach (2002), who gives a range of effective medium models for the physical properties of inclusions of one phase in another phase, as well as the inverse case. As an applied example, Vasseur et al. (2016) found that the elastic properties of coherent versus powdered materials were best scaled by two different effective medium models, and that the transition from one to the other (from coherent to powdered) could be captured by a cross over between models. As a result, in the following we will only discuss the measurements performed on rock samples. Finally, we highlight that the Maxwell equation (Equation (1)), and the effective medium models below (Equations (2) and (3)), consider the total porosity, whereas we have measured the connected porosity of our samples. To assess the suitability of using these models to discuss our experimental data (Figure 5; Tables 2 and 3), we provide a plot of connected porosity as a function of total porosity for numerous 20 mm-diameter cylindrical samples from La Soufrière, Chaos Crags, and Merapi volcano (Figure 6), which shows that there is little to no isolated porosity in the studied materials.

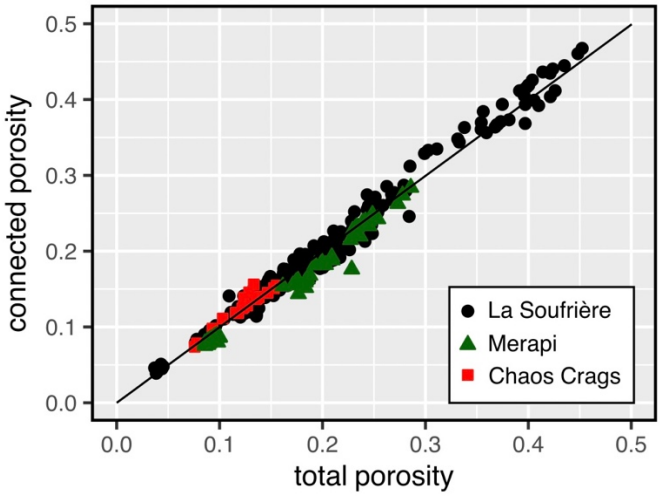

Figure 6. Connected porosity as a function of total porosity for 20 mm-diameter cylindrical samples from La Soufrière, Chaos Crags, and Merapi volcano. The black line shows the 1:1 line, whereat the connected porosity equals the total porosity.

We find that our data for La Soufrière, as well as data for rhyodacites from Chaos Crags and basaltic-andesites from Merapi volcano, are bracketed by curves for which λ_0 is 1.9 and 0.85 W·m^{-1}·K^{-1} (the black lines in Figure 7a). A third curve, which best captures the overall trend of the dataset, is also provided in Figure 7a (for which λ_0 is 1.45 W·m^{-1}·K^{-1}). The effective thermal diffusivity $D(\phi)$ was then determined using,

$$D(\phi) = \frac{\lambda(\phi)}{\rho_s C_p (1-\phi) + \rho_f C_{p,f} \phi}, \quad (2)$$

where ρ_s and ρ_f are the groundmass and pore fluid densities, respectively, and C_p and $C_{p,f}$ are the groundmass and pore fluid specific heat capacity, respectively (Connor et al., 1997). We take values of ρ_f and $C_{p,f}$ of 1.275 kg·m^{-3} and 1.007 kJ·kg^{-1}·K^{-1}, respectively. Values for ρ_s and C_p, guided by our data, were taken as 2650 kg·m^{-3} and 0.8 kJ·kg^{-1}·K^{-1}, respectively. Theoretical curves are provided using the $\lambda(\phi)$ values taken from the three models shown in

Figure 7a (i.e. λ_0 = 1.9, 1.45, and 0.85 W·m^{-1}·K^{-1}; Equation (1); the black lines in Figure 7b). Based on Equation (2), the effective specific heat capacity $C_p(\phi)$ is given by the porosity-weighted average,

$$C_p(\phi) = \frac{\rho_s C_p(1-\phi) + \rho_f C_{p,f}\phi}{\rho_b}, (3)$$

where ρ_b is the bulk sample density, where $\rho_b = \rho_s(1-\phi) + \rho_f\phi$. To plot $C_p(\phi)$, we take the same values outlined above for the different variables (the black line in Figure 7c).

The effective medium models (Equations (1), (2), and (3)) are in reasonable agreement with the data (Figure 7), suggesting that porosity plays an important role in governing their thermal properties (as discussed in Heap et al., 2020a). The scatter in these data, i.e. the reason why even data from the same volcano cannot be described by a single theoretical curve (Figure 7), is the result of factors not considered in Equations (1), (2), and (3), such as differences in the nature of the void space (e.g., pore size, shape, and number density, microcrack density; factors that can vary significantly in volcanic rocks, see the review of Heap and Violay, 2021) and differences in their mineral componentry (e.g., variable alteration intensities and secondary mineral assemblages). The large differences in the alteration of these rocks (Tables 2 and 3), and that the effective medium approaches well describe the relatively unaltered suite of rocks from Ruapehu (Figure 7; Heap et al., 2020a) and Hawai'i (Robertson and Peck, 1974) with variable pore sizes and shapes, suggest that the scatter in the data can be explained by their variable alteration, discussed in the next section.

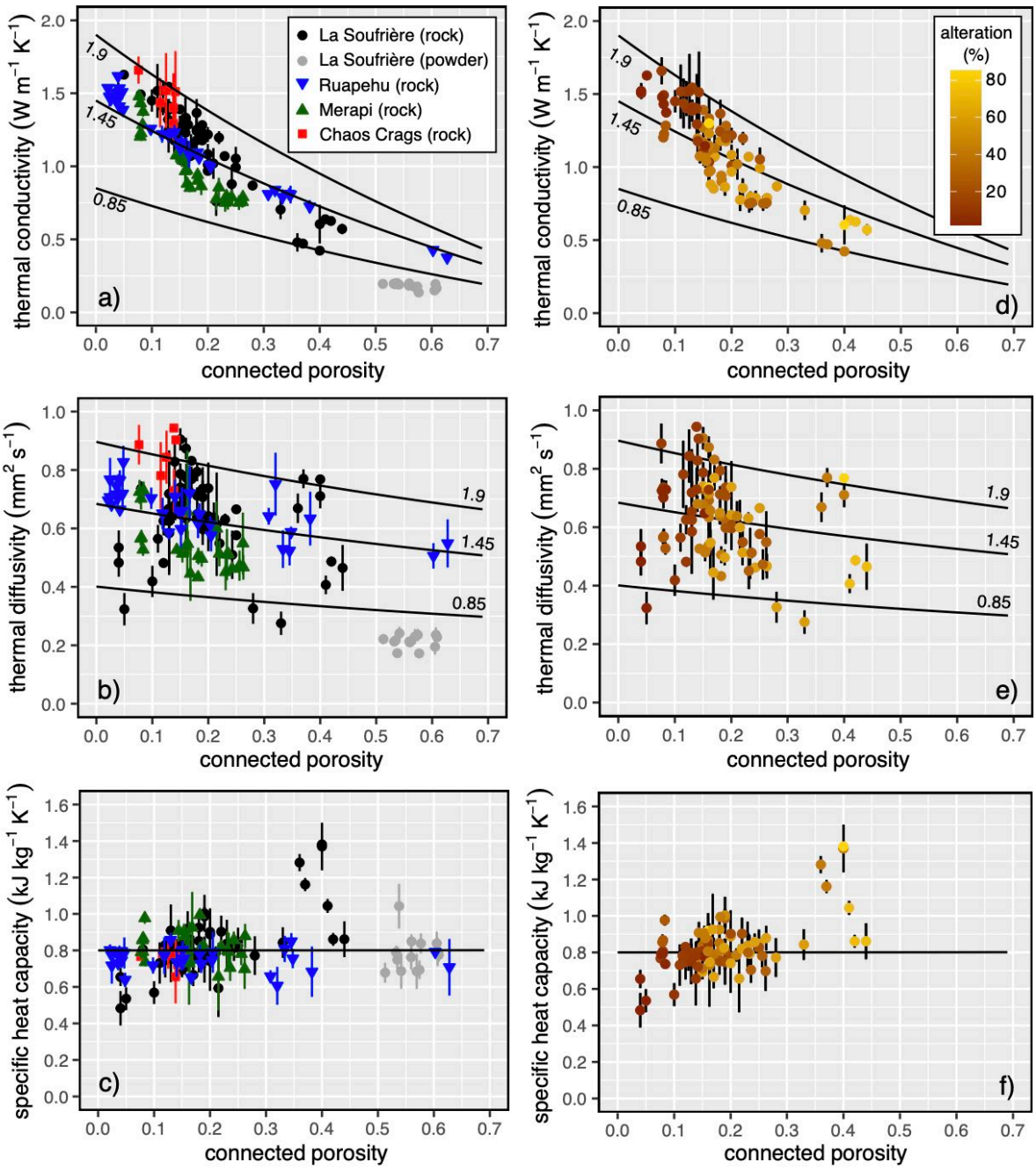

Figure 7. Thermal conductivity (a and d), thermal diffusivity (b and e), and specific heat capacity (c and f) as a function of connected porosity for the samples from La Soufrière de Guadeloupe (Eastern Caribbean), Merapi volcano (Indonesia; data from Heap et al., 2020a), Ruapehu (New Zealand; data from Heap et al., 2020a), and Chaos Crags (USA). In panels (a–c), the symbols and colours differentiate the data from the different volcanoes (La Soufrière de Guadeloupe: black (rocks) and grey circles (powders); Merapi volcano: green triangles;

475 Ruapehu: blue triangles; Chaos Crags: red squares). In panels (d–f), the colour of the symbol
476 (where red and yellow indicate low and high values, respectively) indicates the alteration
477 (percentage of secondary minerals). Numbers next to the modelled curves in panels (a), (b),
478 (d), and (e) indicate the assumed rock groundmass conductivity, λ_0 (in $W \cdot m^{-1} \cdot K^{-1}$). The
479 modelled curves for λ_0 values of 0.85 and 1.9 $W \cdot m^{-1} \cdot K^{-1}$ are designed to bracket the dataset.
480
481 5.2 The influence of alteration on thermal properties
482 To explore the influence of hydrothermal alteration on the thermal properties of volcanic
483 rocks, we plot thermal conductivity, thermal diffusivity, and specific heat capacity as a function
484 of alteration (taken to be the weight percentage of secondary minerals) in Figure 8. We
485 supplement these data with published data for variably-altered basaltic-andesites from Merapi
486 volcano (from Heap et al., 2020a; Table 3) and new data for variably-altered rhyodacites from
487 Chaos Crags (Table 3). The methods used, XRPD to quantify their mineral contents and the
488 Hot Disk® Thermal Constants Analyser to measure their thermal properties, were the same as
489 for the measured materials from La Soufrière (presented in Table 2), adding confidence to direct
490 data comparisons. Similar to the samples from La Soufrière, the secondary mineral assemblages
491 of the rocks from Merapi volcano and Chaos Crags correspond to intermediate to advanced
492 argillic alteration.

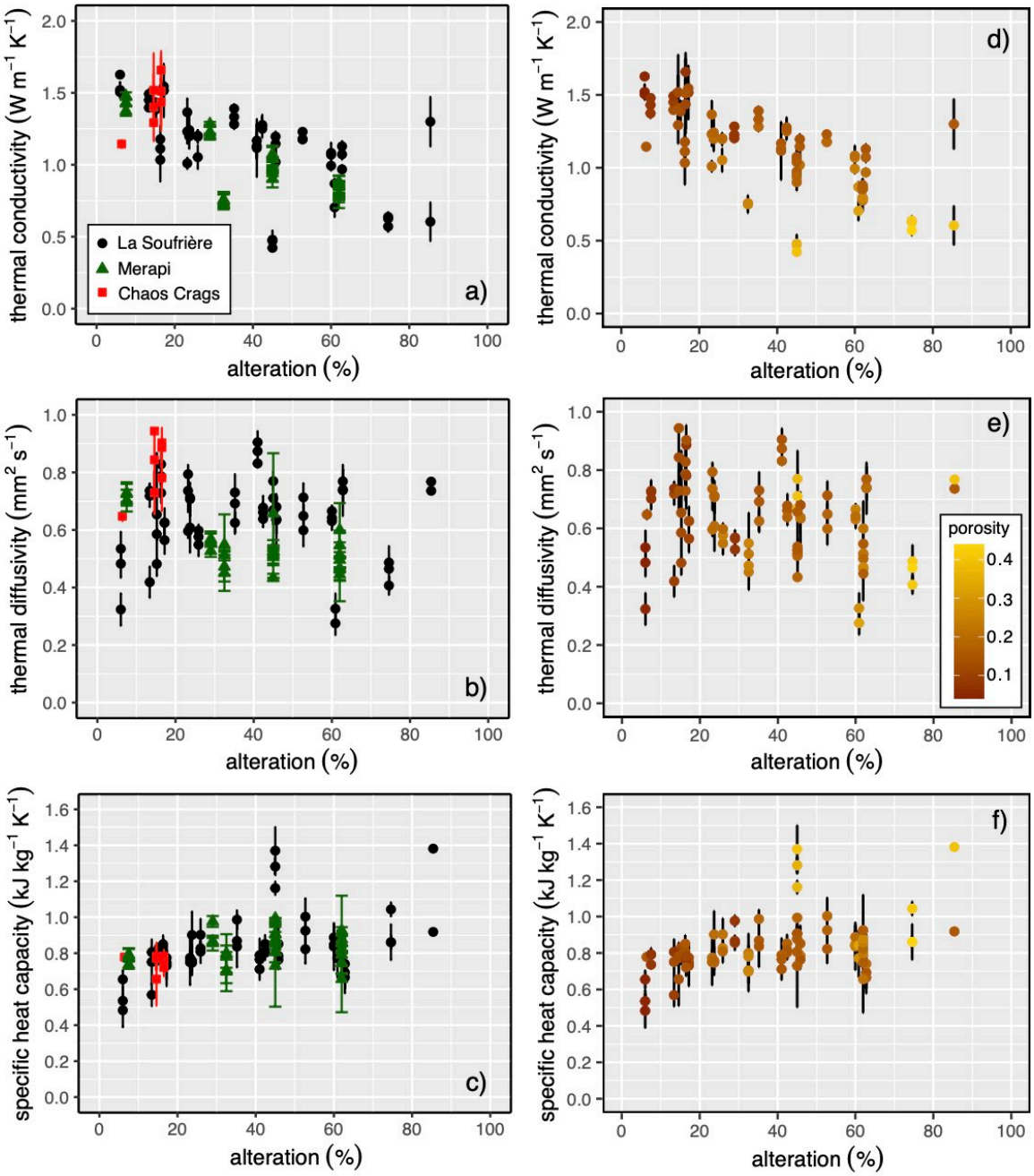

493

494 **Figure 8.** Thermal conductivity (a and d), thermal diffusivity (b and e), and specific heat
495 capacity (c and f) as a function of alteration (percentage of secondary minerals) for the
496 samples from La Soufrière de Guadeloupe (Eastern Caribbean), Merapi volcano (Indonesia;
497 data from Heap et al., 2020a), and Chaos Crags (USA). In panels (a–c), the symbols and
498 colours differentiate the data from the different volcanoes (La Soufrière de Guadeloupe: black
499 (rocks) and grey circles (powders); Merapi volcano: green triangles; Ruapehu: blue triangles;

Chaos Crags: red squares). In panels (d–f), the colour of the symbol (where red and yellow indicate low and high values, respectively) indicates the connected porosity.

The thermal conductivity of the rocks from La Soufrière and Merapi volcano decreases as a function of increasing alteration, from ~1.6 $W \cdot m^{-1} \cdot K^{-1}$ at an alteration of ~1.5 wt.% to ~0.6 $W \cdot m^{-1} \cdot K^{-1}$ at an alteration >75 wt.% (Figure 8a). The thermal conductivity of the rocks from Chaos Crags, on the other hand, increases as alteration increases, from ~1.1 $W \cdot m^{-1} \cdot K^{-1}$ at an alteration of ~6 wt.% to ~1.5 $W \cdot m^{-1} \cdot K^{-1}$ at an alteration of ~15 wt.% (Figure 8a). Although the thermal diffusivity of the rocks from La Soufrière and Merapi volcano does not appear to be influenced by alteration, the thermal diffusivity of the rocks from Chaos Crags increases from ~0.65 to ~0.75−0.95 $mm^2 \cdot s^{-1}$ as alteration increases from ~6 to ~15 wt.% (Figure 8b). The specific heat capacity of all rocks does not appear to be significantly affected by alteration, although there is a slight trend of increasing specific heat capacity with increasing alteration for the rocks from La Soufrière (Figure 8c).

The reasons for the observed changes in thermal properties as a function of hydrothermal alteration (Figure 8) are twofold. First, the thermal properties of the primary and secondary minerals differ (Horai, 1971; Brigaud and Vasseur, 1989; Clauser and Huenges, 1995). Therefore, increasing the proportion of secondary minerals at the expense of the primary minerals will either increase or decrease the thermal properties of a sample, depending on whether the secondary minerals have higher values of thermal conductivity, diffusivity, and specific heat capacity than the primary minerals. Second, hydrothermal alteration can promote either increases in porosity (dissolution) or decreases in porosity (pore- and crack-filling mineral precipitation), a physical property known to influence thermal conductivity (as discussed in the previous section; Figure 5; Robertson and Peck, 1974; Heap et al., 2020a).

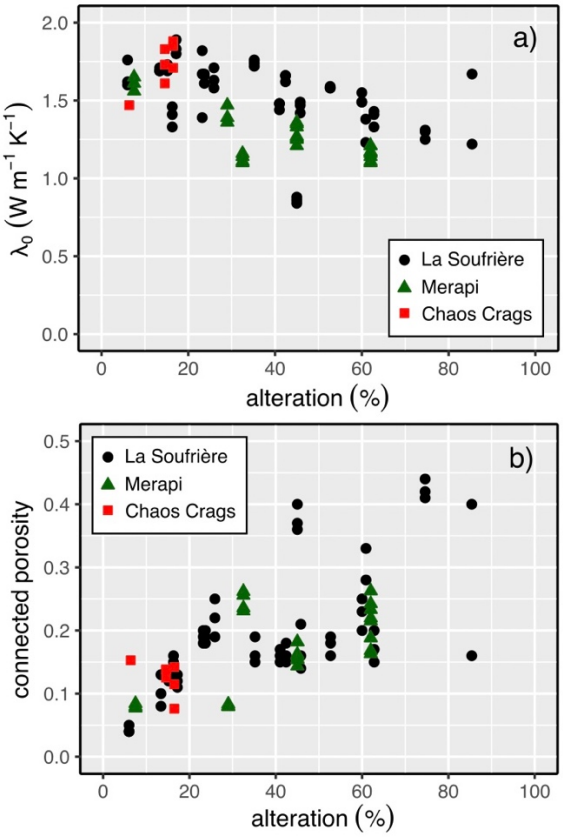

525

526 **Figure 9.** The thermal conductivity of the rock groundmass, λ_0, calculated using Equation (1)
527 (a) and the connected porosity (b) as a function of alteration (percentage of secondary
528 minerals) for the samples from La Soufrière de Guadeloupe (Eastern Caribbean; black
529 circles), Merapi volcano (Indonesia; green triangles; data from Heap et al., 2020a), and Chaos
530 Crags (USA; red squares).

531

532 To explore whether the different thermal properties of secondary minerals, compared to
533 primary minerals, is affecting the thermal properties of the studied rocks, we exploit the fact
534 that Equation (1) shows that λ is only a function of λ_0 (the thermal conductivity of the
535 groundmass) and the porosity, such that we can solve for λ_0 for each sample. The value of λ_0
536 for each sample represents the thermal conductivity of the sample at zero porosity, allowing us
537 to assess solely the influence of alteration on thermal conductivity. λ_0 is plotted as a function
538 of alteration in Figure 9a. Figure 9a shows that λ_0 broadly decreases as a function of alteration

539 for the samples from La Soufrière and Merapi volcano, but appears to increase for the samples
540 from Chaos Crags. The decrease in thermal conductivity as a function of alteration for the
541 samples from La Soufrière and Merapi volcano can be, at least partly, explained by the lower
542 thermal conductivity of the secondary minerals compared to the primary minerals (Horai, 1971;
543 Brigaud and Vasseur, 1989; Clauser and Huenges, 1995). For example, the thermal conductivity
544 of kaolinite, a common replacement mineral in the rocks from La Soufrière (Table 1; Figures 3
545 and 4), is lower that of plagioclase (Horai, 1971; Brigaud and Vasseur, 1989). For the rocks
546 from Chaos Crags, we note that, although smectite and kaolinite have low thermal
547 conductivities (Brigaud and Vasseur, 1989), the high thermal conductivity of cristobalite (~6
548 $W \cdot m^{-1} \cdot K^{-1}$; Kunugi et al., 1972) could explain why their thermal conductivities appear to
549 increase as a function of increasing alteration (Figure 8a).

550 The above analysis suggests that hydrothermal alteration can modify the thermal
551 conductivity of volcanic rock by changing the mineral assemblage. However, alteration can
552 also result in either increases in porosity (dissolution) or decreases in porosity (pore- and crack-
553 filling mineral precipitation), a parameter that we have already established as important in
554 dictating the thermal properties of volcanic rock (Figure 7). To explore whether the observed
555 alteration as resulted in changes to porosity, and therefore thermal properties, we plot alteration
556 as a function of porosity in Figure 9b. We also provide plots in Figure 7 that show thermal
557 conductivity, thermal diffusivity, and specific heat capacity as a function of porosity in which
558 the symbol colour indicates the alteration (Figures 7d, 7e, and 7f). Similarly, in Figures 8d, 8e,
559 and 8f, which show plots of thermal conductivity, thermal diffusivity, and specific heat capacity
560 as a function of alteration, the symbol colour indicates the porosity. Figure 9b shows that
561 porosity increases as a function of alteration for the rocks from La Soufrière and Merapi
562 volcano, but appears to decrease as a function of alteration for the rocks from Chaos Crags.
563 Figures 7d−f and 8d−f also show that the more altered samples are typically the most porous.

Therefore, we could conclude from these data that the changes in thermal properties as a function of alteration (Figure 8a) are also the result of alteration-induced increases (in the case of the rocks from La Soufrière and Merapi volcano) and decreases (in the case of the rocks from Chaos Crags) to the porosity, alongside the changes resulting from modifications to the mineral assemblage (Figure 9a). However, because alteration efficiency is increased by higher fluid-rock ratios (Giggenbach, 1984), another possibility is that the high-porosity rocks collected from La Soufrière and Merapi volcano are simply more altered because they were initially more porous and permeable. We also note that detailed microstructural analysis on the rocks from La Soufrière (Figures 3 and 4; Heap et al., 2021a) and Merapi volcano (Heap et al., 2019, 2021c) shows that not all alteration was associated with mineral dissolution, and that samples from both sample suites show evidence of microcrack- and pore-filling alteration (Figures 3 and 4; Heap et al., 2019, 2021a). Therefore, although we observe changes in the thermal properties of the rocks collected from La Soufrière and Merapi volcano as a function of alteration (Figure 8), it is difficult at present to conclude whether changes in porosity resulting directly from alteration influenced their thermal properties. It appears more likely, due to the abundance of void-filling mineral precipitation (Figures 3 and 4; Heap et al., 2021a), that the trend of increasing porosity with alteration (Figure 9b) is simply the result of increasing alteration efficiency at higher porosity due to an increase in fluid-rock ratio (i.e. higher interfacial surface area). Therefore, in the case of the andesites and basaltic-andesites from La Soufrière and Merapi volcano, it is likely that the decrease in thermal conductivity as a function of alteration (Figure 8a) is the result of the low conductivity of the secondary mineral assemblage (Horai, 1971; Brigaud and Vasseur, 1989; Clauser and Huenges, 1995).

The explanation that higher porosities, and therefore higher fluid-rock ratios, led to more efficient alteration, however, cannot explain the decrease in porosity as alteration is increased from ~6 wt.% to ~15 wt.% in the rocks from Chaos Crags (Figure 9b). Detailed microstructural

589 work on the rocks from Chaos Crags showed that the alteration was manifest as microcrack-
590 and pore-filling mineral precipitation of mainly cristobalite and kaolinite (Heap et al., 2021b).
591 Therefore, in the case of the rhyodacites from Chaos Crags, it is likely that the increase in
592 thermal conductivity (Figure 8a) and thermal diffusivity (Figure 8b) as alteration is increased
593 from ~6 to ~15 wt.% is the result of a combination of the high thermal conductivity of
594 cristobalite and the reduction in porosity as a result of the void-filling mineral precipitation.
595
596 5.3 Volcanological implications
597 The heat flux from an active volcano provides crucial information on volcanic unrest
598 (Jessop al., 2021) and provides an indication as to the likelihood of magmatic and phreatic
599 eruptions (Girona et al., 2021). As a result, processes that can alter the thermal properties of
600 dome- or edifice-forming rocks are of interest to those tasked with interpreting volcano heat
601 flux data. We have shown here that porosity (Figure 7) and alteration (Figure 8) can influence
602 the thermal properties of suites of volcanic rocks (basaltic-andesites, andesites, and rhyodacites)
603 from La Soufrière, Merapi volcano, and Chaos Crags. The main focus of this contribution is
604 the influence of alteration on thermal properties.
605 To explore the influence of alteration on the heat output of a dome, we can provide
606 estimates for the contribution of the heat flux from the dome, q, from conduction alone using
607 Fourier's law,
608
609 $$q = -\lambda \frac{dT}{dz} \approx \lambda \frac{\Delta T}{H}, (4)$$
610
611 where λ is the thermal conductivity, T is the temperature, z is the vertical position in the dome
612 ($z = 0$ is the dome top and $z = H$ is the base of the dome), and ΔT is the difference in
613 temperature between the top and base of the dome. Although in a real volcanic setting, heat

614 may be transported by a number of additional mechanisms that would represent additional terms
615 in Equation (4), here we assume that heat transport is by conduction alone, which allows us to
616 investigate the relative influence of alteration on heat flux. We additionally neglect a
617 temperature-dependence of λ, which is valid at the relatively low temperatures of edifice rocks
618 (Whittington et al., 2009; Romaine et al., 2012) and assume that the dome is homogeneous. We
619 assume at dome height $H = 200$ m, and a temperature difference $\Delta T = 300$ °C. Based on our
620 experimental results (Figure 8a), we consider two scenarios: (1) a scenario in which alteration
621 decreases the thermal conductivity and (2) a scenario in which alteration increases the thermal
622 conductivity. For each scenario, we consider three dome states: (1) unaltered, (2) slightly
623 altered, and (3) altered. For the first scenario we assume thermal conductivities of 1.5, 1, and
624 0.5 $W \cdot m^{-1} \cdot K^{-1}$ for the unaltered, slightly altered, and altered dome, respectively (Figure 7a).
625 And for the second scenario we assume thermal conductivities of 1, 1.25, and 1.5 $W \cdot m^{-1} \cdot K^{-1}$
626 for the unaltered, slightly altered, and altered dome, respectively (Figure 8a). The calculated
627 conductive heat flux for the first scenario are 2.25, 1.5, and 0.75 $W \cdot m^{-2}$, respectively, and 1.5,
628 1.875, and 2.25 $W \cdot m^{-2}$ for the second scenario, respectively. These simple calculations should
629 be considered for illustrative purposes only as they assume (1) that the dome is homogenous in
630 terms of its thermal conductivity, and (2) there is no temperature dependence of thermal
631 conductivity, a factor that can influence the thermal properties of volcanic rocks (Whittington
632 et al., 2009; Romaine et al., 2012). Nevertheless, for conductive heat transport alone, it is clear
633 from Equation (4) that the alteration-dependence of λ will have a linearly proportional impact
634 on q. Our results show that λ can change by up to a factor of three as alteration increases, which
635 will reduce q by a third. More importantly, our results suggest that dynamic changes in q
636 observed directly at volcanoes could represent changes in sub-surface alteration.
637 The mean ground heat flux measured at La Soufrière, for example, was measured to be
638 406 ± 24 $W \cdot m^{-2}$ in 2020 (Jessop et al., 2021). Therefore, although alteration-induced changes

to the thermal conductivity of the dome can influence the measured heat flux, as discussed above, the contribution from conduction is likely much less than that from other heat transport mechanisms, such as the convection of hydrothermal fluids within the core of the edifice; although we note that conduction becomes the dominant mode of heat transfer between the condensation isotherm and the surface (Harris, 2013), and that ongoing work at La Soufrière supports this view (Lebas, 2021). However, changes in porosity resulting from alteration can also modify permeability (Sruoga et al., 2004; Mayer et al., 2016; Heap et al., 2017b, 2019, 2020b; Revil et al., 2020; Kennedy et al., 2020; Heap et al., 2021b; Kanakiya et al., 2021), which can influence the efficiency of the migration of hot fluids up through the dome structure and therefore affect the measured volcano heat flux by increasing or decreasing the influence of convection. Therefore, alteration can influence volcanic heat flux by changing the thermal conductivity of the rocks, as explored in this contribution, and also by changing the ease of convection within the dome by modifying permeability. A full description of heat transfer, in which conduction and convection are solved together, that also incorporates the influence of hydrothermal alteration on thermal properties, porosity, and permeability represents the logical next step in unravelling the influence of alteration on volcano heat flux. Although this complete description currently eludes us, we conclude with the available data that hydrothermal alteration can influence volcano heat flux and should therefore be considered when interpreting heat flux data collected at active volcanoes worldwide.

6 Conclusions

We have provided laboratory measurements of thermal conductivity, thermal diffusivity, and specific heat capacity for variably altered volcanic rocks. These data show that thermal conductivity and thermal diffusivity decrease as a function of porosity, and that specific heat capacity does not change systematically as a function of porosity (as discussed in Heap et

al., 2020a). When plotted as a function of alteration (the percentage of secondary minerals), we find that thermal conductivity decreases for the rocks from La Soufrière and Merapi volcano, but appears to increase for the rocks from Chaos Crags. Although the thermal diffusivity of the rocks from Chaos Crags increases as a function of alteration, the thermal diffusivity of the rocks from La Soufrière and Merapi volcano does not appear to be influenced by alteration. The specific heat capacity is not significantly affected by alteration, although there is a slight trend of increasing specific heat capacity with alteration for the rocks from La Soufrière.

We conclude that the decrease in thermal conductivity as a function of alteration in the rocks from La Soufrière and Merapi volcano is the result of the low conductivity of the secondary mineral assemblage, and that a combination of the high thermal conductivity of cristobalite and the reduction in porosity as a result of the void-filling mineral precipitation can explain the increase in thermal conductivity in the rocks from Chaos Crags.

Although Fourier's law shows that an increase in alteration of a dome or edifice can modify thermal conductivity and therefore heat flux, the contribution from conduction is likely much less than that from other heat transport mechanisms, such as convection (see, for example, Jessop et al., 2021). However, we conclude that not only is it important to be aware that alteration can influence the thermal conductivity of the dome or edifice, but that alteration can also influence permeability and therefore the convection of heat, a factor that can greatly modify the heat flux measured at the volcano.

Because the heat flux of an active volcano provides crucial information about volcanic unrest (Jessop al., 2021; Girona et al., 2021), we conclude that the extent and, importantly, the type of alteration should be routinely monitored. Monitoring can be performed by remote and/or ground-based optical and spectroscopic methods (Crowley and Zimbelman, 1997; John et al., 2008; Darmawan et al., 2018; Kereszturi et al., 2020; Mueller et al., 2021), gas and thermal monitoring (Edmonds et al., 2003; Tamburello et al., 2019; de Moor et al., 2019; Jessop et al.,

2021; Moretti et al., 2020), geological mapping (van Wyk de Vries et al., 2000), magnetic methods (Finn et al., 2007), deformation monitoring (Moretti et al., 2020), near-surface seismic imaging (Amoroso et al., 2018), electrical tomography (Ahmed et al., 2018; Byrdina et al., 2017; Ghorbani et al., 2018; Rosas-Carbajal et al., 2016), and muon tomography (Lesparre et al., 2012; Rosas-Carbajal et al., 2017). A better understanding of hydrothermal alteration, and how alteration can influence the thermal properties, porosity, and permeability of dome- and edifice-forming rock, will allow for a deeper understanding of volcano heat fluxes and therefore the hazards posed by volcanoes with active hydrothermal systems.

Acknowledgements

This work was supported by the TelluS Program of INSU-CNRS ("Assessing the role of hydrothermal alteration on volcanic hazards") and ANR grant MYGALE ("Modelling the phYsical and chemical Gradients of hydrothermal ALteration for warning systems of flank collapse at Explosive volcanoes"), awarded to the first author. M. Heap also acknowledges support from the Institut Universitaire de France (IUF). We thank the IPGP for general funding for the Observatoires Volcanologiques et Sismologiques (OVS), INSU-CNRS for the funding provided by the Service National d'Observation en Volcanologie (SNOV), and the Ministère pour la Transition Ecologique (MTE) for financial support for the monitoring of the instable flank of La Soufrière de Guadeloupe. This study contributes to the IdEx Université de Paris ANR-18-IDEX-0001. We thank Tomaso Esposti Ongaro, Gilles Morvan, and Christophe Nevado. Material collection from Chaos Crags as permitted by the United States National Park Service (study: LAVO-00050; permit: LAVO-2019-SCI-0010), and we thank Kelly Russell, Stephan Kolzenburg, Lori Kennedy, Martin Harris, and Michael Clynne for their help and support. This is Laboratory of Excellence /ClerVolc /contribution n° 506. We thank two reviewers for constructive comments that helped improve this manuscript.

CRediT author statement

Michael J. Heap: Conceptualization; Methodology; Formal analysis; Investigation; Resources; Writing - Original draft; Visualization; Supervision; Project administration; Funding acquisition

David Jessop: Conceptualization; Investigation; Resources

Marina Rosas-Carbajal: Investigation; Resources; Project administration; Funding acquisition

Jean-Christophe Komorowski: Investigation; Resources; Project administration; Funding acquisition

H. Albert Gilg: Investigation

Nadège Aron: Investigation

Margaux Buscetti: Investigation

Laura Gential: Investigation

Margaux Goupil: Investigation

Mathilde Masson: Investigation

Lucie Hervieu: Investigation

Alexandra R.L. Kushnir: Methodology; Supervision

Patrick Baud: Investigation; Resources

Lucille Carbillet: Investigation; Resources

Amy G. Ryan: Investigation; Resources

Roberto Moretti: Resources; Project administration

References

738 Ahmed, A. S., Revil, A., Byrdina, S., Coperey, A., Gailler, L., Grobbe, N., ... & Hogg, C.
739 (2018). 3D electrical conductivity tomography of volcanoes. Journal of Volcanology and
740 Geothermal Research, 356, 243-263.
741 Allard, P., Aiuppa, A., Beauducel, F., Gaudin, D., Di Napoli, R., Calabrese, S., ... &
742 Tamburello, G. (2014). Steam and gas emission rate from La Soufriere volcano,
743 Guadeloupe (Lesser Antilles): implications for the magmatic supply during degassing
744 unrest. Chemical Geology, 384, 76-93.
745 Amoroso, O., Festa, G., Bruno, P. P., D'Auria, L., De Landro, G., Di Fiore, V., ... & Zollo, A.
746 (2018). Integrated tomographic methods for seismic imaging and monitoring of volcanic
747 caldera structures and geothermal areas. Journal of Applied Geophysics, 156, 16-30.
748 Annen, C., Pichavant, M., Bachmann, O., & Burgisser, A. (2008). Conditions for the growth of
749 a long-lived shallow crustal magma chamber below Mount Pelee volcano (Martinique,
750 Lesser Antilles Arc). Journal of Geophysical Research: Solid Earth, 113(B7).
751 Annen, C. (2017). Factors affecting the thickness of thermal aureoles. Frontiers in Earth
752 Science, 5, 82.
753 Bagdassarov, N., & Dingwell, D. (1994). Thermal properties of vesicular rhyolite. Journal of
754 Volcanology and Geothermal Research, 60(2), 179-191.
755 Bergmann, J., Friedel, P., & Kleeberg, R. (1998). BGMN—a new fundamental parameters
756 based Rietveld program for laboratory X-ray sources, its use in quantitative analysis and
757 structure investigations. CPD Newsletter, 20(5).
758 Bloomberg, S., Werner, C., Rissmann, C., Mazot, A., Horton, T., Gravley, D., ... & Oze, C.
759 (2014). Soil CO2 emissions as a proxy for heat and mass flow assessment, Taupō
760 Volcanic Zone, New Zealand. Geochemistry, Geophysics, Geosystems, 15(12), 4885-
761 4904.
762 Boudon, G., Semet, M. P., & Vincent, P. M. (1987). Magma and hydrothermally driven sector
763 collapses: The 3100 and 11,500 y. BP eruptions of la Grande Decouverte (la Soufriere)
764 volcano, Guadeloupe, French West Indies. Journal of Volcanology and Geothermal
765 Research, 33(4), 317-323.
766 Bouligand, C., Coutant, O., & Glen, J. M. (2016). Sub-surface structure of La Soufrière of
767 Guadeloupe lava dome deduced from a ground-based magnetic survey. Journal of
768 Volcanology and Geothermal Research, 321, 171-181.
769 Brigaud, F., & Vasseur, G. (1989). Mineralogy, porosity and fluid control on thermal
770 conductivity of sedimentary rocks. Geophysical Journal International, 98(3), 525-542.
771 Brombach, T., Marini, L., & Hunziker, J. C. (2000). Geochemistry of the thermal springs and
772 fumaroles of Basse-Terre Island, Guadeloupe, Lesser Antilles. Bulletin of Volcanology,
773 61(7), 477-490.
774 Brothelande, E., Finizola, A., Peltier, A., Delcher, E., Komorowski, J. C., Di Gangi, F., ... &
775 Legendre, Y. (2014). Fluid circulation pattern inside La Soufrière volcano (Guadeloupe)
776 inferred from combined electrical resistivity tomography, self-potential, soil temperature
777 and diffuse degassing measurements. Journal of Volcanology and Geothermal Research,
778 288, 105-122.
779 Bruce, P. M., & Huppert, H. E. (1989). Thermal control of basaltic fissure eruptions. Nature,
780 342(6250), 665-667.
781 Byrdina, S., Friedel, S., Vandemeulebrouck, J., Budi-Santoso, A., Suryanto, W., Rizal, M. H.,
782 & Winata, E. (2017). Geophysical image of the hydrothermal system of Merapi volcano.
783 Journal of Volcanology and Geothermal Research, 329, 30-40.
784 Carrigan, C. R. (1984). Time and temperature dependent convection models of cooling
785 reservoirs: Application to volcanic sills. Geophysical Research Letters, 11(8), 693-696.

786 Carrigan, C. R., Schubert, G., & Eichelberger, J. C. (1992). Thermal and dynamical regimes of
787 single-and two-phase magmatic flow in dikes. Journal of Geophysical Research: Solid
788 Earth, 97(B12), 17377-17392.
789 Chiodini, G., Granieri, D., Avino, R., Caliro, S., Costa, A., & Werner, C. (2005). Carbon
790 dioxide diffuse degassing and estimation of heat release from volcanic and hydrothermal
791 systems. Journal of Geophysical Research: Solid Earth, 110(B8).
792 Clauser, C., & Huenges, E. (1995). Thermal conductivity of rocks and minerals. Rock physics
793 and phase relations: a handbook of physical constants, 3, 105-126.
794 Connor, C. B., Lichtner, P. C., Conway, F. M., Hill, B. E., Ovsyannikov, A. A., Federchenko,
795 I., ... & Taran, Y. A. (1997). Cooling of an igneous dike 20 yr after intrusion. Geology,
796 25(8), 711-714.
797 Crowley, J. K., & Zimbelman, D. R. (1997). Mapping hydrothermally altered rocks on Mount
798 Rainier, Washington, with airborne visible/infrared imaging spectrometer (AVIRIS) data.
799 Geology, 25(6), 559-562.
800 Darmawan, H., Walter, T. R., Brotopuspito, K. S., & Nandaka, I. G. M. A. (2018).
801 Morphological and structural changes at the Merapi lava dome monitored in 2012–15
802 using unmanned aerial vehicles (UAVs). Journal of Volcanology and Geothermal
803 Research, 349, 256-267.
804 Dehn, J., Dean, K., & Engle, K. (2000). Thermal monitoring of North Pacific volcanoes from
805 space. Geology, 28(8), 755-758.
806 de Moor, J. M., Stix, J., Avard, G., Muller, C., Corrales, E., Diaz, J. A., ... & Fischer, T. P.
807 (2019). Insights on hydrothermal-magmatic interactions and eruptive processes at Poás
808 Volcano (Costa Rica) from high-frequency gas monitoring and drone measurements.
809 Geophysical Research Letters, 46(3), 1293-1302.
810 Döbelin, N., & Kleeberg, R. (2015). Profex: a graphical user interface for the Rietveld
811 refinement program BGMN. Journal of applied crystallography, 48(5), 1573-1580.
812 Edmonds, M., Oppenheimer, C., Pyle, D. M., Herd, R. A., & Thompson, G. (2003). SO2
813 emissions from Soufrière Hills Volcano and their relationship to conduit permeability,
814 hydrothermal interaction and degassing regime. Journal of Volcanology and Geothermal
815 Research, 124(1-2), 23-43.
816 Feuillard, M., Allègre, C. J., Brandeis, G., Gaulon, R., Le Mouel, J. L., Mercier, J. C., ... &
817 Semet, M. P. (1983). The 1975–1977 crisis of La Soufrière de Guadeloupe (FWI): a still-
818 born magmatic eruption. Journal of Volcanology and Geothermal Research, 16(3-4), 317-
819 334.
820 Fialko, Y. A., & Rubin, A. M. (1999). Thermal and mechanical aspects of magma emplacement
821 in giant dike swarms. Journal of Geophysical Research: Solid Earth, 104(B10), 23033-
822 23049.
823 Finn, C. A., Deszcz-Pan, M., Ball, J. L., Bloss, B. J., & Minsley, B. J. (2018). Three-
824 dimensional geophysical mapping of shallow water saturated altered rocks at Mount
825 Baker, Washington: Implications for slope stability. Journal of Volcanology and
826 Geothermal Research, 357, 261-275.
827 Fujii, N., & Osako, M. (1973). Thermal diffusivity of lunar rocks under atmospheric and
828 vacuum conditions. Earth and Planetary Science Letters, 18(1), 65-71.
829 Gaudin, D., Beauducel, F., Allemand, P., Delacourt, C., & Finizola, A. (2013). Heat flux
830 measurement from thermal infrared imagery in low-flux fumarolic zones: Example of the
831 Ty fault (La Soufrière de Guadeloupe). Journal of Volcanology and Geothermal
832 Research, 267, 47-56.
833 Ghorbani, A., Revil, A., Coperey, A., Ahmed, A. S., Roque, S., Heap, M. J., ... & Viveiros, F.
834 (2018). Complex conductivity of volcanic rocks and the geophysical mapping of
835 alteration in volcanoes. Journal of Volcanology and Geothermal Research, 357, 106-127.

836 Giggenbach, W. F. (1984). Mass transfer in hydrothermal alteration systems—a conceptual
837 approach. Geochimica et Cosmochimica Acta, 48(12), 2693-2711.
838 Girona, T., Realmuto, V., & Lundgren, P. (2021). Large-scale thermal unrest of volcanoes for
839 years prior to eruption. Nature Geoscience, 14(4), 238-241.
840 Gustavsson, M., Karawacki, E., & Gustafsson, S. E. (1994). Thermal conductivity, thermal
841 diffusivity, and specific heat of thin samples from transient measurements with hot disk
842 sensors. Review of Scientific Instruments, 65(12), 3856-3859.
843 Gustafsson, S. E. (1991). Transient plane source techniques for thermal conductivity and
844 thermal diffusivity measurements of solid materials. Review of scientific instruments,
845 62(3), 797-804.
846 Hammerschmidt, U., & Sabuga, W. (2000). Transient hot strip (THS) method: uncertainty
847 assessment. International Journal of Thermophysics, 21(1), 217-248.
848 Harlé, P., Kushnir, A. R., Aichholzer, C., Heap, M. J., Hehn, R., Maurer, V., ... & Duringer, P.
849 (2019). Heat flow density estimates in the Upper Rhine Graben using laboratory
850 measurements of thermal conductivity on sedimentary rocks. Geothermal Energy, 7(1),
851 1-36.
852 Harris, A. J., Blake, S., Rothery, D. A., & Stevens, N. F. (1997). A chronology of the 1991 to
853 1993 Mount Etna eruption using advanced very high resolution radiometer data:
854 Implications for real-time thermal volcano monitoring. Journal of Geophysical Research:
855 Solid Earth, 102(B4), 7985-8003.
856 Harris, A. J. L., Pilger, E., Flynn, L. P., Garbeil, H., Mouginis-Mark, P. J., Kauahikaua, J., &
857 Thornber, C. (2001). Automated, high temporal resolution, thermal analysis of Kilauea
858 volcano, Hawai'i, using GOES satellite data. International Journal of Remote Sensing,
859 22(6), 945-967.
860 Harris, A. (2013). Thermal remote sensing of active volcanoes: a user's manual. Cambridge
861 University Press.
862 Heap, M. J., & Kennedy, B. M. (2016). Exploring the scale-dependent permeability of fractured
863 andesite. Earth and Planetary Science Letters, 447, 139-150.
864 Heap, M. J., Violay, M., Wadsworth, F. B., & Vasseur, J. (2017a). From rock to magma and
865 back again: the evolution of temperature and deformation mechanism in conduit margin
866 zones. Earth and Planetary Science Letters, 463, 92-100.
867 Heap, M. J., Kennedy, B. M., Farquharson, J. I., Ashworth, J., Mayer, K., Letham-Brake, M.,
868 ... & Dingwell, D. B. (2017b). A multidisciplinary approach to quantify the permeability
869 of the Whakaari/White Island volcanic hydrothermal system (Taupo Volcanic Zone, New
870 Zealand). Journal of Volcanology and Geothermal Research, 332, 88-108.
871 Heap, M. J., Troll, V. R., Kushnir, A. R., Gilg, H. A., Collinson, A. S., Deegan, F. M., ... &
872 Walter, T. R. (2019). Hydrothermal alteration of andesitic lava domes can lead to
873 explosive volcanic behaviour. Nature Communications, 10(1), 1-10.
874 Heap, M. J., Kushnir, A. R., Vasseur, J., Wadsworth, F. B., Harlé, P., Baud, P., ... & Deegan,
875 F. M. (2020a). The thermal properties of porous andesite. Journal of Volcanology and
876 Geothermal Research, 398, 106901.
877 Heap, M. J., Gravley, D. M., Kennedy, B. M., Gilg, H. A., Bertolett, E., & Barker, S. L. (2020b).
878 Quantifying the role of hydrothermal alteration in creating geothermal and epithermal
879 mineral resources: the Ohakuri ignimbrite (Taupō Volcanic Zone, New Zealand). Journal
880 of Volcanology and Geothermal Research, 390, 106703.
881 Heap, M. J., Baumann, T. S., Rosas-Carbajal, M., Komorowski, J. C., Gilg, H. A., Villeneuve,
882 M., ... & Reuschlé, T. (2021a). Alteration-induced volcano instability at La Soufrière de
883 Guadeloupe (Eastern Caribbean). Journal of Geophysical Research: Solid Earth,
884 e2021JB022514.

885 Heap, M. J., Baumann, T., Gilg, H. A., Kolzenburg, S., Ryan, A. G., Villeneuve, M., ... &
886 Clynne, M. A. (2021b). Hydrothermal alteration can result in pore pressurization and
887 volcano instability. Geology, https://doi.org/10.1130/G49063.1.
888 Heap, M. J., Wadsworth, F. B., Heng, Z., Xu, T., Griffiths, L., Velasco, A. A., ... & Deegan, F.
889 M. (2021c). The tensile strength of volcanic rocks: Experiments and models. Journal of
890 Volcanology and Geothermal Research, 418, 107348.
891 Heap, M. J., & Violay, M. E. (2021). The mechanical behaviour and failure modes of volcanic
892 rocks: a review. Bulletin of Volcanology, 83(5), 1-47.
893 Hincks, T. K., Komorowski, J. C., Sparks, S. R., & Aspinall, W. P. (2014). Retrospective
894 analysis of uncertain eruption precursors at La Soufrière volcano, Guadeloupe, 1975–77:
895 volcanic hazard assessment using a Bayesian Belief Network approach. Journal of
896 Applied Volcanology, 3(1), 1-26.
897 Hofmeister, A. M. (2019). Measurements, mechanisms, and models of heat transport. Elsevier.
898 Horai, K., Simmons, G., Kanamori, H., & Wones, D. (1970). Thermal diffusivity, conductivity
899 and thermal inertia of Apollo 11 lunar material. Geochimica et Cosmochimica Acta
900 Supplement, 1, 2243.
901 Horai, K. I. (1971). Thermal conductivity of rock-forming minerals. Journal of Geophysical
902 Research, 76(5), 1278-1308.
903 Irvine, T. N. (1970). Heat transfer during solidification of layered intrusions. I. Sheets and sills.
904 Canadian Journal of Earth Sciences, 7(4), 1031-1061.
905 Jessop, D. E., Moune, S., Moretti, R., Gibert, D., Komorowski, J. C., Robert, V., ... & Burtin,
906 A. (2021). A multi-decadal view of the heat and mass budget of a volcano in unrest: La
907 Soufrière de Guadeloupe (French West Indies). Bulletin of Volcanology, 83(3), 1-19.
908 John, D. A., Sisson, T. W., Breit, G. N., Rye, R. O., & Vallance, J. W. (2008). Characteristics,
909 extent and origin of hydrothermal alteration at Mount Rainier Volcano, Cascades Arc,
910 USA: Implications for debris-flow hazards and mineral deposits. Journal of Volcanology
911 and Geothermal Research, 175(3), 289-314.
912 Kanakiya, S., Adam, L., Rowe, M. C., Lindsay, J. M., & Esteban, L. (2021). The role of tuffs
913 in sealing volcanic conduits. Geophysical Research Letters, e2021GL095175.
914 Kennedy, B. M., Farquhar, A., Hilderman, R., Villeneuve, M. C., Heap, M. J., Mordensky, S.,
915 ... & Reuschlé, T. (2020). Pressure controlled permeability in a conduit filled with
916 fractured hydrothermal breccia reconstructed from ballistics from Whakaari (White
917 Island), New Zealand. Geosciences, 10(4), 138.
918 Kereszturi, G., Schaefer, L. N., Miller, C., & Mead, S. (2020). Hydrothermal Alteration on
919 Composite Volcanoes: Mineralogy, Hyperspectral Imaging, and Aeromagnetic Study of
920 Mt Ruapehu, New Zealand. Geochemistry, Geophysics, Geosystems, 21(9),
921 e2020GC009270.
922 Komorowski, J.-C., Boudon, G., Semet, M., Beauducel, F., Anténor-Habazac, C., Bazin, S., &
923 Hammmouya, G. (2005). Guadeloupe. In: Volcanic Atlas of the Lesser Antilles (Eds:
924 Lindsay, J., Robertson, R., Shepherd, J., & Ali, S.), University of the French West Indies,
925 Seismic Research Unit, pp. 65-102.
926 Komorowski, J.-C., Hincks, T., Sparks, R., Aspinall, W., & CASAVA ANR Project
927 Consortium. (2015). Improving crisis decision-making at times of uncertain volcanic
928 unrest (Guadeloupe, 1976). In: Global Volcanic Hazards and Risk (Eds: Loughlin, S.C.,
929 Sparks, R.S.J., Brown, S.K., Jenkins, S.F., & Vye-Brown, C), Cambridge University
930 Press, pp 255-261.
931 Kunugi, M., Soga, N., Sawa, H., & Konishi, A. (1972). Thermal conductivity of cristobalite.
932 Journal of the American Ceramic Society, 55(11), 580-580.

933 Lebas, F. (2021). Etude du dégazage et de la perte de chaleur du système hydrothermal de La
934 Soufrière de Guadeloupe : implications pour la surveillance volcanique. Master thesis.
935 Université de Paris-IPGP.
936 Le Friant, A., Boudon, G., Komorowski, J. C., Heinrich, P., & Semet, M. P. (2006). Potential
937 flank-collapse of Soufrière volcano, Guadeloupe, Lesser Antilles? Numerical simulation
938 and hazards. Natural Hazards, 39(3), 381.
939 Lesparre, N., Gibert, D., Marteau, J., Komorowski, J. C., Nicollin, F., & Coutant, O. (2012).
940 Density muon radiography of La Soufriere of Guadeloupe volcano: comparison with
941 geological, electrical resistivity and gravity data. Geophysical Journal International,
942 190(2), 1008-1019.
943 Mannini, S., Harris, A. J., Jessop, D. E., Chevrel, M. O., & Ramsey, M. S. (2019). Combining
944 Ground-and ASTER-Based Thermal Measurements to Constrain Fumarole Field Heat
945 Budgets: The Case of Vulcano Fossa 2000–2019. Geophysical Research Letters, 46(21),
946 11868-11877.
947 Mattsson, T., Burchardt, S., Almqvist, B. S., & Ronchin, E. (2018). Syn-emplacement
948 fracturing in the Sandfell laccolith, eastern Iceland—Implications for rhyolite intrusion
949 growth and volcanic hazards. Frontiers in Earth Science, 6, 5.
950 Mayer, K., Scheu, B., Montanaro, C., Yilmaz, T. I., Isaia, R., Aßbichler, D., & Dingwell, D. B.
951 (2016). Hydrothermal alteration of surficial rocks at Solfatara (Campi Flegrei):
952 Petrophysical properties and implications for phreatic eruption processes. Journal of
953 Volcanology and Geothermal Research, 320, 128-143.
954 Mielke, P., Nehler, M., Bignall, G., & Sass, I. (2015). Thermo-physical rock properties and the
955 impact of advancing hydrothermal alteration—A case study from the Tauhara geothermal
956 field, New Zealand. Journal of Volcanology and Geothermal Research, 301, 14-28.
957 Mielke, P., Weinert, S., Bignall, G., & Sass, I. (2016). Thermo-physical rock properties of
958 greywacke basement rock and intrusive lavas from the Taupo Volcanic Zone, New
959 Zealand. Journal of Volcanology and Geothermal Research, 324, 179-189.
960 Mielke, P., Bär, K., & Sass, I. (2017). Determining the relationship of thermal conductivity and
961 compressional wave velocity of common rock types as a basis for reservoir
962 characterization. Journal of Applied Geophysics, 140, 135-144.
963 Moretti, R., Komorowski, J. C., Ucciani, G., Moune, S., Jessop, D., de Chabalier, J. B., ... &
964 Chaussidon, M. (2020). The 2018 unrest phase at La Soufrière of Guadeloupe (French
965 West Indies) andesitic volcano: Scrutiny of a failed but prodromal phreatic eruption.
966 Journal of Volcanology and Geothermal Research, 393, 106769.
967 Mueller, D., Bredemeyer, S., Zorn, E., De Paolo, E., & Walter, T. R. (2021). Surveying
968 fumarole sites and hydrothermal alteration by unoccupied aircraft systems (UAS) at the
969 La Fossa cone, Vulcano Island (Italy). Journal of Volcanology and Geothermal Research,
970 413, 107208.
971 Nabelek, P. I., Hofmeister, A. M., & Whittington, A. G. (2012). The influence of temperature-
972 dependent thermal diffusivity on the conductive cooling rates of plutons and temperature-
973 time paths in contact aureoles. Earth and Planetary Science Letters, 317, 157-164.
974 Nicollin, F., Gibert, D., Beauducel, F., Boudon, G., & Komorowski, J. C. (2006). Electrical
975 tomography of La Soufrière of Guadeloupe Volcano: Field experiments, 1D inversion
976 and qualitative interpretation. Earth and Planetary Science Letters, 244(3-4), 709-724.
977 Norton, D., & Knight, J. (1977). Transport phenomena in hydrothermal systems: cooling
978 plutons. Am. J. Sci.;(United States), 277.
979 Peruzzetto, M., Komorowski, J. C., Le Friant, A., Rosas-Carbajal, M., Mangeney, A., &
980 Legendre, Y. (2019). Modeling of partial dome collapse of La Soufrière of Guadeloupe
981 volcano: implications for hazard assessment and monitoring. Scientific reports, 9(1), 1-
982 15.

Revil, A., Coperey, A., Heap, M. J., & Carbillet, L. (2020). A geophysical index to map alteration, permeability, and mechanical properties within volcanoes. Application to the soft volcanic rocks from Whakaari/White Island (New Zealand). Journal of Volcanology and Geothermal Research, 401, 106945.

Robertson, E. C., & Peck, D. L. (1974). Thermal conductivity of vesicular basalt from Hawaii. Journal of Geophysical Research, 79(32), 4875-4888.

Romine, W. L., Whittington, A. G., Nabelek, P. I., & Hofmeister, A. M. (2012). Thermal diffusivity of rhyolitic glasses and melts: effects of temperature, crystals and dissolved water. Bulletin of volcanology, 74(10), 2273-2287.

Rosas-Carbajal, M., Komorowski, J. C., Nicollin, F., & Gibert, D. (2016). Volcano electrical tomography unveils edifice collapse hazard linked to hydrothermal system structure and dynamics. Scientific Reports, 6(1), 1-11.

Rosas-Carbajal, M., Jourde, K., Marteau, J., Deroussi, S., Komorowski, J. C., & Gibert, D. (2017). Three-dimensional density structure of La Soufrière de Guadeloupe lava dome from simultaneous muon radiographies and gravity data. Geophysical Research Letters, 44(13), 6743-6751.

Ryan, A. G., Heap, M. J., Russell, J. K., Kennedy, L. A., & Clynne, M. A. (2020). Cyclic shear zone cataclasis and sintering during lava dome extrusion: Insights from Chaos Crags, Lassen Volcanic Center (USA). Journal of Volcanology and Geothermal Research, 401, 106935.

Salaün, A., Villemant, B., Gérard, M., Komorowski, J. C., & Michel, A. (2011). Hydrothermal alteration in andesitic volcanoes: trace element redistribution in active and ancient hydrothermal systems of Guadeloupe (Lesser Antilles). Journal of Geochemical Exploration, 111(3), 59-83.

Sruoga, P., Rubinstein, N., & Hinterwimmer, G. (2004). Porosity and permeability in volcanic rocks: a case study on the Serie Tobífera, South Patagonia, Argentina. Journal of Volcanology and Geothermal Research, 132(1), 31-43.

Stevenson, J. A., & Varley, N. (2008). Fumarole monitoring with a handheld infrared camera: Volcán de Colima, Mexico, 2006–2007. Journal of Volcanology and Geothermal Research, 177(4), 911-924.

Tamburello, G., Moune, S., Allard, P., Venugopal, S., Robert, V., Rosas-Carbajal, M., ... & Moretti, R. (2019). Spatio-temporal relationships between fumarolic activity, hydrothermal fluid circulation and geophysical signals at an arc volcano in degassing unrest: La Soufrière of Guadeloupe (French West Indies). Geosciences, 9(11), 480.

Torquato, S., & Haslach Jr, H. W. (2002). Random heterogeneous materials: microstructure and macroscopic properties. Appl. Mech. Rev., 55(4), B62-B63.

Tsang, S. W., Lindsay, J. M., Coco, G., Wysocki, R., Lerner, G. A., Rader, E., ... & Kennedy, B. (2019). The heating of substrates beneath basaltic lava flows. Bulletin of Volcanology, 81(11), 1-14.

van Wyk de Vries, B., Kerle, N., & Petley, D. (2000). Sector collapse forming at Casita volcano, Nicaragua. Geology, 28(2), 167-170.

Vasseur, J., Wadsworth, F. B., Lavallée, Y., & Dingwell, D. B. (2016). Dynamic elastic moduli during isotropic densification of initially granular media. Geophysical Journal International, 204(3), 1721-1728.

Vélez, M. I., Blessent, D., Córdoba, S., López-Sánchez, J., Raymond, J., & Parra-Palacio, E. (2018). Geothermal potential assessment of the Nevado del Ruiz volcano based on rock thermal conductivity measurements and numerical modeling of heat transfer. Journal of South American Earth Sciences, 81, 153-164.

Villemant, B., Hammouya, G., Michel, A., Semet, M. P., Komorowski, J. C., Boudon, G., & Cheminée, J. L. (2005). The memory of volcanic waters: shallow magma degassing

revealed by halogen monitoring in thermal springs of La Soufrière volcano (Guadeloupe, Lesser Antilles). Earth and Planetary Science Letters, 237(3-4), 710-728.

Villemant, B., Komorowski, J. C., Dessert, C., Michel, A., Crispi, O., Hammouya, G., ... & De Chabalier, J. B. (2014). Evidence for a new shallow magma intrusion at La Soufrière of Guadeloupe (Lesser Antilles): insights from long-term geochemical monitoring of halogen-rich hydrothermal fluids. Journal of Volcanology and Geothermal Research, 285, 247-277.

Whittington, A. G., Hofmeister, A. M., & Nabelek, P. I. (2009). Temperature-dependent thermal diffusivity of the Earth's crust and implications for magmatism. Nature, 458(7236), 319-321.

Wooster, M. J., & Rothery, D. A. (1997). Thermal monitoring of Lascar Volcano, Chile, using infrared data from the along-track scanning radiometer: a 1992–1995 time series. Bulletin of Volcanology, 58(7), 566-579.

Wooster, M. J., Wright, R., Blake, S., & Rothery, D. A. (1997). Cooling mechanisms and an approximate thermal budget for the 1991–1993 Mount Etna lava flow. Geophysical Research Letters, 24(24), 3277-3280.

Wright, R., & Flynn, L. P. (2004). Space-based estimate of the volcanic heat flux into the atmosphere during 2001 and 2002. Geology, 32(3), 189-192.

Wright, R., Flynn, L. P., Garbeil, H., Harris, A. J., & Pilger, E. (2004). MODVOLC: near-real-time thermal monitoring of global volcanism. Journal of Volcanology and Geothermal Research, 135(1-2), 29-49.

Weydt, L. M., Ramírez-Guzmán, Á. A., Pola, A., Lepillier, B., Kummerow, J., Mandrone, G., ... & Sass, I. (2021). Petrophysical and mechanical rock property database of the Los Humeros and Acoculco geothermal fields (Mexico). Earth System Science Data, 13(2), 571-598.

Zimmerman, R. W. (1989). Thermal conductivity of fluid-saturated rocks. Journal of Petroleum Science and Engineering, 3(3), 219-227.